TOKYO METROPOLITAN UNIVERSITY

DOCTORAL THESIS

# Control of Energy Transfer Reaction on the Inorganic Nano-Sheet for an Artificial Light-Harvesting System

March, 2017

Yuta Ohtani

# Preface

This thesis is based on the studies which were worked under the guidance of Professor Shinsuke Takagi at Department of Applied Chemistry, Graduate Course of Urban Environmental Sciences, Tokyo Metropolitan University.

March, 2017

Yuta Ohtani

Department of Applied Chemistry,
Graduate Course of Urban Environmental Sciences,
Tokyo Metropolitan University
1-1 Minami-ohsawa, Hachiohji,
Tokyo, 192-0364, JAPAN

Contents

# 1. Introduction

## 1-1. Purpose

Fossil fuels are limited resources that continue to be utilized. In order to avoid exhaustion of these resources, studies utilizing solar energy have been conducted. Solar energy is mainly converted to chemical energy and electric energy. With absorption and propagation of light energy being the initial processes for such conversion, the efficiency of these processes must be sufficiently high in order to allow efficient use of solar energy.

Our research group has been studying artificial photosynthesis, the reaction of which converts light energy into chemical energy. The photosynthetic system in nature is mainly divided into a light-harvesting system (LHS) and a photochemical reaction system, with the former being involved in the initial process of energy conversion. In order to improve the initial process, we aimed to construct an artificial LHS. This LHS has three functions: expansion of the absorption wavelength range, transfer of light energy to the photochemical reaction center, and control of excitation frequency and excitation energy. We thus set out to examine and improve each function, and constructed an excitation energy transfer system using the organic/inorganic complex.

## 1-2. Light Conversion Reaction

Sunlight energy is used for $CO_2$ reduction and water oxidation during photosynthesis in green plants[1–6]; these reactions convert solar energy to chemical energy. These reactions were evaluated by their conversion efficiency ($\eta_C$) using the equation $\eta_C = J_g \mu_{pro} \phi_{con}/S$.[11] Here, $J_g$ is the absorbed photon flux (photons $s^{-1}$ $m^{-2}$), $\mu_{pro}$ is the chemical potential of the product (J $photon^{-1}$), $\phi_{con}$ is the quantum yield of conversion of absorbed photons into products, and $S$ is the total incident solar energy (W $m^{-2}$). $\eta_C$ signifies the importance of the photon absorption step in the sequence of photosynthesis; therefore, an artificial LHS has been studied to improve this step.

## 1-3. Photosynthetic Reaction

In the photosynthetic reaction, the absorbed solar energy is used in the synthesis of sugar and oxygen from carbon dioxide and water:

$$6CO_2 + 12\ H_2O \rightarrow C_6H_{12}O_6 + 6O_2 + 6\ H_2O$$

Many researchers have attempted to mimic the photosynthetic system in order to use sunlight energy. The photosynthetic system has an LHS and a photoreaction center, that is, its structure mainly consists of an LHS and photosystems I and II (PS I and II, respectively).[1–6] The LHS has several important functions in the photosynthetic system, namely, increase of the absorption wavelength range, dissipation of excess excitation energy, and concentration of absorbed photons in PS I and II. The LHS of purple bacteria is composed of dye molecules such as carotenoids and bacteriochlorophylls.[6–10] Carotenoids in the LHS absorb energy at 450–540 nm, which is higher than that absorbed by bacteriochlorophylls. The excitation energy is transferred to bacteriochlorophylls, and the utilizable sunlight energy in the bacterial system is increased by carotenoids. Carotenoids dissipate approximately 50% of the absorbed energy through an internal conversion process, depending on the light intensity. This process is one of the mechanisms that protects against excess excitation energy. In purple bacteria, approximately 200 dye molecules that comprise the LHS surround the reaction centers,[1] forming a circular array. Since the excitation energy efficiently transfers within the ring and between rings, the LHS can transfer photoenergy efficiently and frequently to PS I and II. Through this light harvesting system, the reaction center increases the light absorption cross section by about 100 times.[1] One of the most important roles of the LHS is concentration of the weak photon flux,

which enables the photochemical reaction of multielectron conversion. In an artificial multielectron conversion system, frequent supply of electrons or photons to the catalyst within the lifetime of an oxidized or reduced catalyst is necessary because an oxidized or reduced catalyst has short lifetime. This difficulty is known as the photon-flux-density problem.[12] Thus, an artificial LHS is crucial to the realization of an artificial photosynthetic system, as is the case with natural photosynthetic systems. This delocalization of the excitation energy and the highly efficient energy transfer reaction between the ring structures are necessary for the light harvesting system.

## 1-4. Artificial LHS

LHS absorbs sunlight and increases the excitation frequency of the reaction center (RC). One of the most important functions of the LHS is concentrating the solar photon density, which increases the excitation frequency. One method of realizing an artificial LHS is the delocalization of excitation energy using assembled dyes. Miyatake et al. (1999, Photochemistry and Photobiology) proposed the use of a zinc–chlorine associate as a supramolecular light-harvesting antenna.[13]

Efficient energy transfer reactions have been achieved in artificial LHSs using covalently linked systems and dendrimer systems.[14–22] Kobuke et al. found that a supramolecular assembly of zinc–porphyrin derivatives can function as an efficient artificial LHS.[22] In this system, excitation-energy hopping (5.3 ± 0.6 ps) is similarly fast as that of a natural system. Inagaki et al. (2009, Angewante Chemistry International Edition)[23] constructed an LHS by using organic mesoporous silica. Inagaki et al. introduced dyes into a mesoporous silica skeleton to form films and powder with high energy efficiency (almost 100%) at very high densities (56 and 125 donor molecules, respectively, for every acceptor molecule). They thus succeeded in constructing an LHS.[23, 24] However, using a dye that absorbs at long wavelength (600 to 750 nm) is difficult since the size of the dye that can be introduced into the mesoporous silica in this system is limited.

The above studies reveal that energy migration between chromophores plays a very important role in efficient energy transfer during light harvesting.

## 1-5. Energy Transfer Reaction[25]

Intermolecular energy transfer occurs when molecules in the excited state interact. The magnitude (β) of the interaction is expressed by the following equation:

$$\beta = < \psi_{initial} | \mathcal{H}'(r_1, r_2) | \psi_{final} >$$

where $\psi$ is the electron wavefunction, $\mathcal{H}'(r_1, r_2)$ is the Hamiltonian of the electrostatic interaction, and $r_i$ is nuclear configuration of molecular $i$.

**· Strong Interaction**

If the wavefunctions of the electronic states of the molecules strongly interact, then excitation migration may occur before nuclear repositioning of the excited molecules. One example of this phenomenon is associate formation, in which the aggregate interacts with the electronic wavefunction in the ground state and assumes a state in which the excited state is split into two. Another example is excimer formation. Since these phenomena take one electronic state with multiple molecules, the intermolecular excitation is completely delocalized.

**· Weak Interaction**

When the interaction is weak, all electronic states of the molecule do not interact, but interaction occurs between vibrational levels of the molecule. The oscillation structure in the absorption band splits, and energy transfer occurs on the same scale as molecular oscillation. Since the magnitude of the interaction until this point is greater than the energy difference between the vibration levels, the absorption spectrum of the molecule is affected.

**· Very Weak Interaction**

β is smaller than the vibration level width. Thus, the probability of energy transfer (W) is expressed as the transition probability equation (Fermi's golden rule):

$$W = \frac{2\pi}{\hbar}\beta^2\rho$$

where $\rho$ represents the level density of the final state (1/3 in the case of triplets). $\hbar$ is Dirac's constant. The mechanism of energy transfer varies with the effect of the interaction on β. For a dipole–dipole interaction, the equation for the electrostatic interaction, $\beta^2 = \kappa^2|\mu_1|^2|\mu_2|^2/n^4R^6$, is appropriate. $\kappa$ is the orientation parameter, $n$ is the refractive index of the bulk medium, $R$ is the intermolecular distance. Substituting this into the above equation and replacing it with quantitative parameters yields the Förster equation:

$$W = \frac{9000 \ln 10\, \kappa^2 \phi_D}{128\pi^5 n^4 N \tau_D R^6} \int f_1\ (\upsilon)\varepsilon_2\ (\upsilon)d\upsilon$$

where $\phi_D$ is the fluorescence quantum yield of energy donor, $N$ is the Avogadro constant, $\tau_D$ is the excited singlet lifetime of donor. Electron exchange interactions occur alongside the dipole interaction. When the intermolecular distances are very close, wavefunctions of electrons exchange:

$$\beta = \langle\psi_1^*(r_1)\psi_2\ (r_2)\theta_1^*(1)\theta_2\ (2)|\mathcal{H}'\ (r_1,r_2)|\psi_1\ (r_1)\psi_2^*(r_2)\theta_1\ (1)\theta_2^*(2)\rangle$$

$$-\langle\psi_1^*(r_1)\psi_2\ (r_2)\theta_1^*(1)\theta_2\ (2)|\mathcal{H}'\ (r_1,r_2)|\psi_2^*(r_1)\psi_1\ (r_2)\theta_2^*(1)\theta_1\ (2)\rangle$$

where θ is a spin function. The first term represents the Coulomb integral and has values only when $\theta_1^*(1) = \theta_1\ (1)$ and $\theta_2\ (2) = \theta_2^*(2)$. However, the first term is 0 in the case of energy transfer between triplets because the above condition is unsatisfied. Here, the second term takes on a value

because $\theta_1^*(1) = \theta_2^*(2)$ and $\theta_2\ (1) = \theta_1\ (2)$. The second term, which represents exchange integration, depends on the overlap of electron clouds of the molecule. This second term may be expressed as a quantitative parameter:

$$W = \frac{2\pi}{\hbar} Z^2 \int f_1\ (\upsilon)\varepsilon_2\ (\upsilon)d\upsilon$$

where $f_1\ (\upsilon)$ is the emission spectrum and $\varepsilon_2\ (\upsilon)$ is the absorption spectrum, both of which are normalized to 1. Here, the mechanism is commonly considered as a Dexter-type energy transfer. Z is a parameter that is proportional to the exchange integral, and the corresponding approximation is $Z^2 = exp\ (-2RL)$, where L is a constant.

**· Energy Transfer Reaction between Homogenous Molecules**

To examine the reaction between donor molecules, Gfeller et al. (1997, JPCB)[26] investigated the energy migration reaction between homogeneous molecules using molecules such as pyronine and oxonine incorporated in micropores. They showed that energy migration theoretically occurs in the Förster mechanism.

## 1-6. Clay Minerals[27]

Clay minerals generally are layered silicates that consist of tetrahedral sheets and octahedral sheets. The structures of the sheets are shown in Figure 1-1. Tetrahedral sheets are mainly composed of tetrahedrons that have $Si^{4+}$ or $Al^{3+}$ at the center and oxygen at the apex (Figure 1-2). The tetrahedrons are connected to each other by sharing an adjacent apex, as shown in Figure 1-1. The octahedral sheets consist of octahedrons of six coordinate complexes between $O^{2-}$ or $OH^{-}$ and cations such as $Al^{3+}$, $Mg^{2+}$, and $Fe^{2+}$ (Figure 1-2), with each octahedron edge shared (Figure 1-1).

In this study, saponite in the smectite group is used as clay mineral. Saponite has negative charges that are generated on the surface by isomorphous substitution of $Al^{3+}$ for $Si^{4+}$ in the tetrahedral sheet (Figure 1-1). Water molecules, metal ions, and organic molecules can be incorporated in between layers, which combine tetrahedral and octahedral sheets.

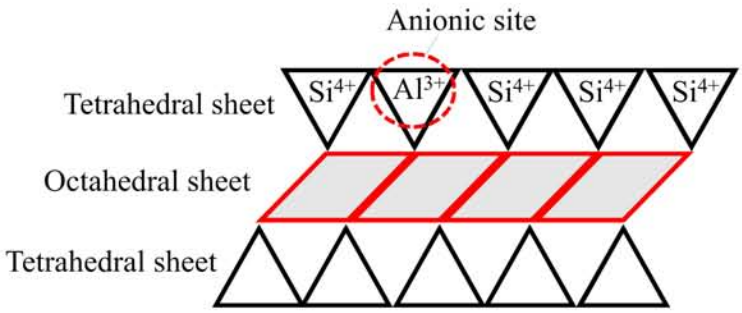


Figure 1-1. Structure of the layered silicate

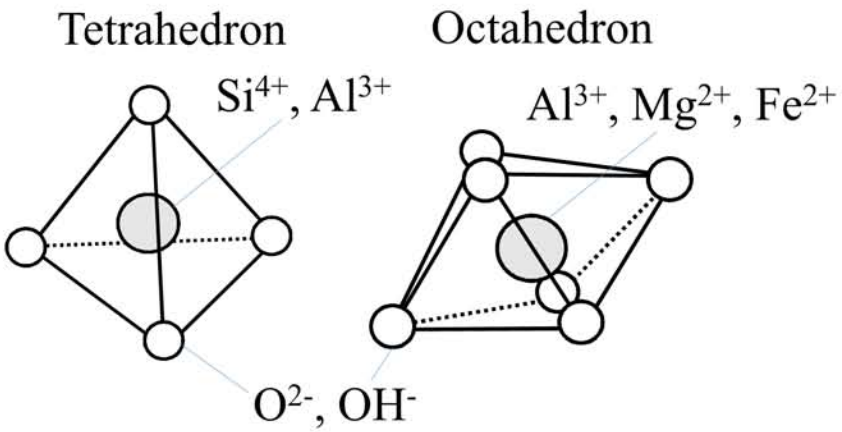


Figure 1-2. Tetrahedral and octahedral structure in layered silicate

## 1-7. Clay–Dye Complexes

We expect that clay minerals can be ideal host materials for constructing structures of dye assemblies for efficient photochemical reactions. Clay minerals are inorganic materials that have negatively charged sites on the flat surface.[27, 28] Photochemical behaviors of organic dyes/clay complexes have been examined by several groups.[28–37, 40–46] Despite reports of unique photochemical properties and reactions,[28–32] the photoactivity of dyes on the clay surface tends to be low because of their aggregation behavior. Nevertheless, we successfully prepared unique porphyrin/clay complexes in which the porphyrin molecules adsorb on the clay surface without aggregation even at high dye loadings. This non-aggregation behavior takes place when the distance between intramolecular cations of dyes match well the negatively charged sites on the clay surface. We term this phenomenon the "size-matching effect".[29–32, 34–36] By using this unique phenomenon, we achieved efficient energy transfer systems for artificial light harvesting.[29–32] Recently, we examined various organic dyes other than porphyrins used as guest dyes.

# 2. Experimental

***• Materials***

*meso*-Tetra (*N*-methyl-4-pyridyl) porphine tetrachloride (*p*-TMPyP) and *meso*-Tetra (*N*-methyl-3-pyridyl) porphine tetrachloride (*m*-TMPyP) were purchased from Frontier Scientific. Water was deionized with an ORGANO BB-5A system (PF filter × 2 + G-10 column). Water was deionized with an ORGANO BB-5A system (PF filter × 2 + G-10 column). The saponite clay used in this experiment was Sumecton SA (SSA), which was received from Kunimine Industries Co. Ltd. The stoichiometric formula is $[(Si_{7.20}Al_{0.80})(Mg_{5.97}Al_{0.03})\ O_{20}\ (OH)_4]^{-0.77}(Na_{0.49}Mg_{0.14})^{+0.77}$, the surface area is 750 $m^2\ g^{-1}$, and the cationic exchange capacity (CEC) is 99.7 meq/100 g.[28] On the basis of these values, the average area per anionic site is calculated to be 1.25 $nm^2$, and thus the average distance between anionic sites on the clay surface is estimated to be 1.2 nm, on the basis of the assumption of a hexagonal array. The SSA was used after purification.

***• Analysis***

Absorption spectra at section 3 and 5 were measured with Shimadzu UV-3150 spectrophotometer. Absorption spectra at section 4 were measured with Shimadzu UV-2600 spectrophotometer. The corrected fluorescence spectra at section 3 and 4 were measured with Jasco FP-6500 spectrofluorometer. The corrected fluorescence spectra at section 5 were measured with Jasco FP-6600 spectrofluorometer. In absorption measurements, a quartz cell was used for aqueous clay/dye solution. In fluorescence measurements, a plastic cell (PMMA) was used for aqueous clay/dye solutions.

TG/DTA measurements were carried out with a Shimadzu DTG-60H analyzer to determine the water content of the dyes and clay. According to TG measurement. Molecular weight of SSA and dyes was corrected according to the water content.

The fluorescence lifetime at section 3-1 was measured by a Hamamatsu Photonics C4780 ps fluorescence lifetime measurement system. The excitation light source of the C4780 was a laser diode (406 nm, 71 ps fwhm, 1 kHz). The laser flux was reduced with neutral density filters to avoid nonlinear effects. Time-resolved fluorescence measurements at section 3-2, 4 and 5 were conducted under a photon-counting condition (Hamamatsu Photonics, C4334 streak scope, connected with CHROMEX 250IS polychrometer) with EKSPLA PG-432 optical parametric generator (430 nm, 25-ps FWHM, 20 μJ, 1kHz) pumped by the third harmonic radiation of $Nd^{3+}$-YAG laser, EKSPLA PL2210JE (355 nm, 25-ps FWHM, 300 μJ, 1kHz). The laser flux was reduced with neutral density filters to avoid multiphoton absorption processes and nonlinear effects. The time-resolved fluorescence spectra were not corrected, thus, the obtained spectral shape was not same to that of the steady state fluorescence spectroscopy even for the same condition.

• ***Purification of clay***

SSA (2.1 g) was dispersed into water (200 ml), and the colloidal solution was stood for 9 days. Then, the supernatant liquid (150 ml) was decanted, and SSA was separated by centrifugation (18000 rpm, 10 hours, 10°C). The supernatant was removed and deionized water was added to it. After standing for 1 day, SSA was separated by centrifugation (18000 rpm, 5 hours, 10°C) again. The supernatant was removed, and SSA was collected by filtration with PTFE membrane (0.45 μm, Millipore) (1.0 g, Yield

48%)

・***Preparation methods for the dye/clay complexes***

Under these experimental conditions, the clay sheets exist in a form of individually exfoliated sheets and the obtained solution was substantially transparent in UV-vis. region.

・***Preparation for the dye/clay complex for absorption spectra***

The dye/clay complex was typically prepared by mixing of the aqueous clay solution and the respective aqueous dye solution under stirring. The dye loadings were changed by adjusting the concentration of dye. The concentration of clay was always kept constant.

・***Preparation for the dye/clay complex for fluorescence spectra***

The dye/clay complex was typically prepared by mixing of the aqueous clay solution and the respective aqueous dye solution under stirring. The clay loadings were changed by adjusting the concentration of clay. The concentration of dye was always kept constant.

# 3. Extension of Absorption Wavelength Region

By extending the absorption wavelength region, it is possible to improve the utilization efficiency of sunlight, and the choices of subsequent reactions will increase. I set out to combine various dyes and to perform stepwise energy transfer reaction.

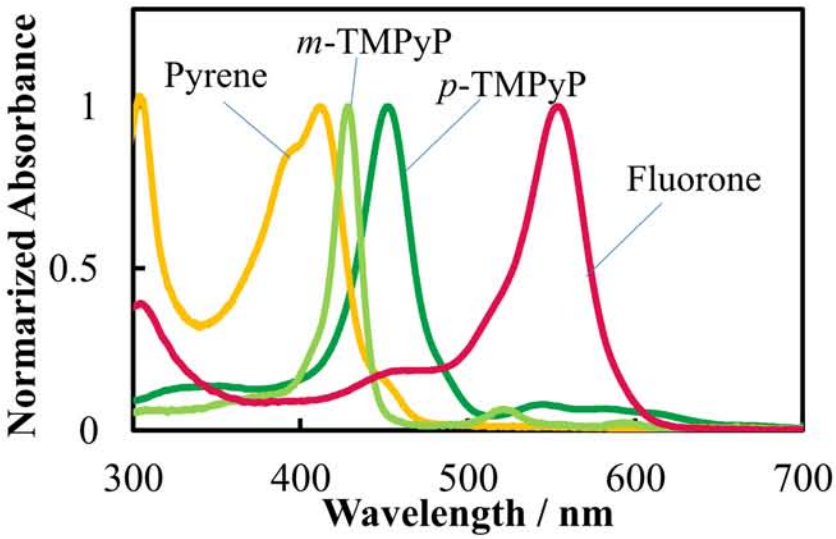

# 3-1. *p*-2,4,5,7-tetrakis(*N*-methyl pyridinium-4-yl)-6-pottasiumoxy-3-fluorone (Fluorone)

## 3-1-1. Introduction

Xanthene dyes such as fluoresceins, eosins, fluorones and rhodamines are useful dyes as fluorescent probes and a dye for a dye laser.[38, 39] They have a high fluorescence quantum yield and an enough long fluorescence lifetime as photo-functional dyes. Although fluorescent rhodamine-clay complex has been investigated,[40-46] rhodamine molecule easily forms their aggregates on the clay surface at high dye loadings.[40-43] In this study, we designed and synthesized the novel tetra cationic xanthene dye (Fluorone: Figure 3-1) and investigated its adsorption and photochemical behavior with and without clay in water.

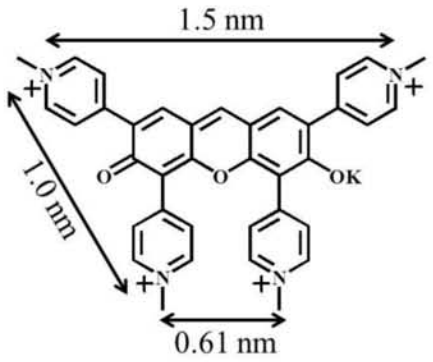


Figure 3-1. The structure of *p*-2,4,5,7-tetrakis(*N*-methyl pyridinium-4-yl)-6-pottasiumoxy-3-fluorone (Fluorone). The inter-cationic distance calculated by PM6 method is shown by arrows.

## 3-1-2. Experimental Section

• ***Materials***

*p*-2,4,5,7-tetrakis(*N*-methylpyridinium-4-yl)-6-pottasiumoxy-3-fluorone (Fluorone; Figure 1) was synthesized as shown in Figure 3-2. 2,4,5,7-Tetrabromo-6-hydroxy-3-fluorone was purchased from Spectra Group. 4-(4,4,5,5-Tetramethyl-1,3,2- dioxaborolan-2-yl)pyridine, pottasium carbonic acid and tetrakis (triphenylphosphine)palladium were purchased from Tokyo Chemical Industry Co. Ltd. dimethylformamide (DMF), dimethylsulfoxide (DMSO) and iodomethane were purchased from Kanto Chemical Co. Ltd.

• ***Synthesis of p-2,4,5,7(pyridinyl)-6- pottasiumoxy -3-fluorone***

2,4,5,7-tetrabromo-6-hydroxy-3-fluorone (76.3 mg), 4-(4,4,5,5-tetramethyl-1,3,2- dioxaborolan- 2-yl) pyridine (519.4 mg) and pottasium carbonic acid (1068.7 mg) were added to degassed DMF (8 mL) and water (2 mL) under $N_2$. After tetrakis（triphenylphosphine） palladium (49.5 mg) was added to the mixture, it was heated to 80°C for 70 hours. 40 hours later, (4,4,5,5-tetramethyl-1,3,2-dioxaborolan-2-yl） pyridine (200.2 mg) and tetrakis（triphenylphosphine） padium (21.3 mg) were added. After cooling, the solvent was evaporated at room temperature and the black solid was obtained. Then, it was dissolved in methanol and removed from reaction flask. The solution was evaporated. Yielded solid was purified by column chromatography (silica gel; acetonitrile : triethylamine : water = 90 : 5 : 5 v/v/v) and, the fraction where $R_f$ value is 0.27 was collected. After evaporation, dichloromethane (100 mL × 3) was added and the mixture was extracted with water (100 mL). Water phase was collected, and was evaporated. The obtained crude product was purified twice by preparative

TLC (silica gel; Acetonitrile : Triethylamine : water = 90 : 5 : 5 v/v/v). Silica gel where the product adsorbed on was collected, and the product was extracted with methanol. Silica gel was removed from the solution by filtration (PTFE, 0.1 μm, Millipore), and the filtrate was evaporated. The obtained solid was put on a membrane filter (PTFE, 0.1 μm, Millipore), and was washed by methanol. The black-purple solid was obtained (28.0 mg, Yield 35%). $^1$H-NMR: (DMSO-$d_6$, 500 MHz) δ: 8.51(dd, 4H, 5.97, 1.53 Hz), 8.28(dd, 4H, 6.30, 1.59 Hz), 8.17(s, 1H), 7.75(s, 2H), 7.74(dd, 4H, 6.30, 1.53 Hz), 7.21(dd, 4H, 5.99, 1.50 Hz) ppm.

***• Synthesis of p-2,4,5,7-tetrakis(N-methylpyridinium-4-yl)-6-pottasiumoxy-3-fluorone (Fluorone)***

Synthesized *p*-2,4,5,7(pyridinyl)-6-pottasiumoxy-3-fluorone (25.2 mg) was dissolved in degassed DMSO (8 mL), and iodomethane (1.8 g) was added to the solution. The mixture was stirred for 2 hours at room temperature. After stirring, the solution was transferred to other flask and degassed DMSO (2 mL) was added to it. To the solution, acetone (2 L) was slowly added. The precipitates were collected by filtration (PTFE, 0.1 μm, Millipore) and were dispersed into ethanol by sonication. The precipitates were collected by filtration (PTFE, 0.1 μm, Millipore). The solid was dissolved into water (50 mL) and chloroform (50 mL × 3) was added to the solution. The product was extracted with water and the water phase was collected. The solvent was removed by evaporation and the obtained solid was heated to 60°C in vacuum for 4 hours. The black-purple solid was obtained (9.7 mg, Yield 18%). $^1$H-NMR: ($D_2O$, 500 MHz) δ: 8.75(d, 4H, 6.63 Hz), 8.72(s, 1H), 8.65(d, 4H, 6.63 Hz), 8.34(d, 4H, 6.63 Hz),

8.23(s, 2H), 8.09(d, 4H, 6.63 Hz), 4.45(s, 6H), 4.39(s, 6H) ppm. Elemental analysis: Calculated for $C_{37}H_{31}N_4I_4KO_3$ - $4.7H_2O$: C, 36.69; H, 3.36; N, 4.62; Found: C, 36.41; H, 3.11; N, 4.45.

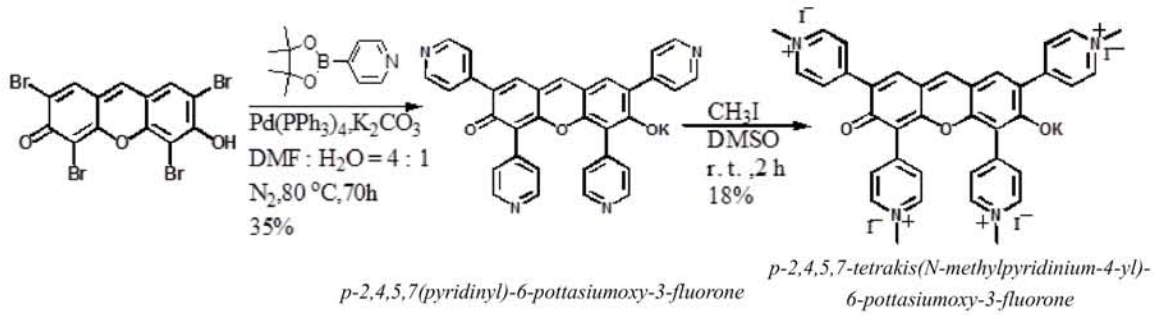


Figure 3-2. Synthetic scheme of Fluorone.

- ***Analysis***

X-Ray Fluorescence (XRF) was observed with Rigaku ZSX 100E under vacuum.

- ***Preparation for Fluorone/clay complex for measuring XRF***

XRF was measured for detection of iodide ion in Fluorone/clay complex, only clay film, and glass substrate.

- ***Preparation of Fluorone/clay complex film***

The glass substrate (cover glass (Matsunami , C024241), 24 mm × 24 mm, thickness is 0.145 ± 0.025 mm) was treated in sulfuric acid (Kanto Chemical, 96%) overnight at room temperature. Then, the glass substrate was washed with enough water. 1 mL of Sumecton SA (SSA, Kunimine) dispersion (1 g $L^{-1}$) and 0.5 mL of Fluorone solution (0.10 mmol $L^{-1}$) were added in 1 mL of water. The mixture was filtered through a PTFE membrane filter (pore size = 0.1 μm). The Fluorone/clay complex thin film was obtained by transferring the residue upon the glass substrate. The thin film was dried up under vacuum overnight.

・***Preparation of the clay film (reference sample)***

1 mL of SSA dispersion (1 g $L^{-1}$) and 0.5 mL of 1, 4-Dioxane (Kanto chemical, 99.5%) were added in 1 mL of water. The mixture was filtered through a PTFE membrane filter (pore size = 0.1 μm). The clay thin film was obtained by transferring the filtrated material upon the glass substrate. The obtained thin film was dried up under vacuum overnight.

・***Preparation of the clay film with KI (reference sample)***

10.9 μL of KI water solution (4.6 mmol $L^{-1}$) was put on the prepared clay film. The amount of KI corresponds to $5.0 \times 10^{-8}$ mol of Fluorone. This film was dried up under atmosphere overnight.

### 3-1-3. Results and discussions

・ ***Adsorption behavior of Fluorone on the clay surface***

Adsorption behavior of Fluorone on the clay surface was examined by the measurement of absorption spectra. At first, absorption spectra of Fluorone with and without clay is shown in Figure 3-3. The absorption and fluorescence maxima are 525 nm and 565 nm, respectively. The absorption coefficient of Fluorone without clay at 525 nm is $9.14 \times 10^4$ $M^{-1}$ $cm^{-1}$. The absorption coefficient of Fluorone with clay at 565 nm is $8.90 \times 10^4$ $M^{-1}$ $cm^{-1}$.

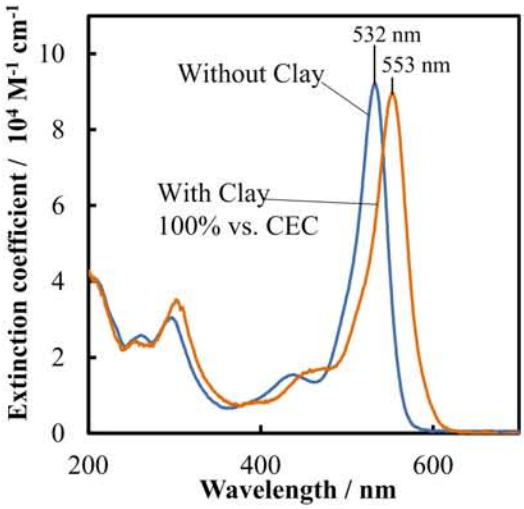


Figure 3-3. Absorption spectra of Fluorone with and without clay in water.

Next, absorption spectra of Fluorone on the clay surface were observed at various dye loadings (10 – 260% vs. CEC) as shown in Figure 3-4. While the spectra retained same shape below 140% vs. CEC adsorption, the observed spectral shape changed above 140%. This indicates that the new species were appeared above 140% vs. CEC adsorption. The $\lambda_{max}$ (525 nm) and the spectral shape of new species above 140% are same as that of Fluorone in water without clay. Thus, the long-wavelength absorption at 553 nm was the component of the adsorbed Fluorone on the clay surface, and newly superimposed short-wavelength absorption at 525 nm was component of non-adsorbed Fluorone in bulk solution. All spectra can be expressed by the combination of the component of the adsorbed Fluorone on the clay surface and it of non-adsorbed Fluorone. This type of spectral shift to longer wavelength (532 → 553

nm) upon the complex formation with clay is frequently observed for aromatic compounds. According to the literature[34], the $\lambda_{max}$ shift of Fluorone upon adsorption on the clay surface is due to the expansion of conjugated system by the planarization of the molecular structure on the clay surface.

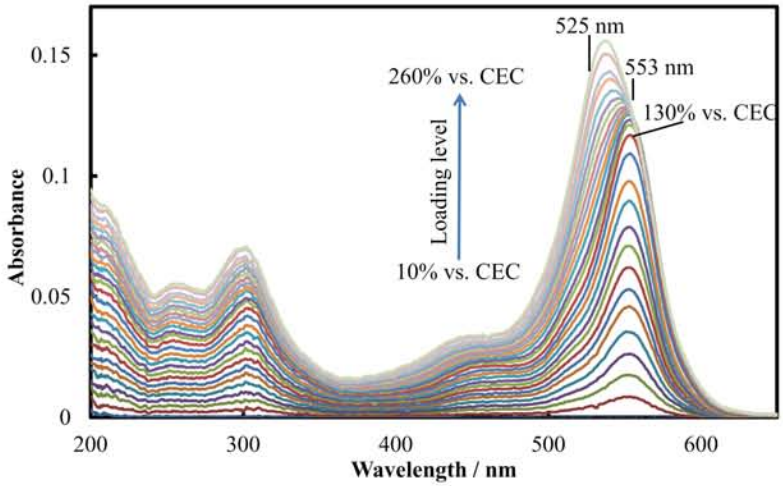


Figure 3-4. Absorption spectra of Fluorone/clay complexes at various concentrations of Fluorone. The loading levels were 10~260% vs. CEC of the clay at intervals at 10% vs. CEC in water. The concentration of clay was 4.0 mg $L^{-1}$.

The Lambert-Beer plot for Fluorone/clay complexes at 525 and 553 nm is shown in Figure 3-5. As shown in Figure 3-5, the linearity of the plot was observed below 134% vs. CEC of the clay. Thus, it turns out that the Fluorone does not form aggregate in the ground sate and exists as a single molecule for 0-134% vs. CEC, although typical dye molecules cannot exist as a single molecule on the clay even at low density condition.

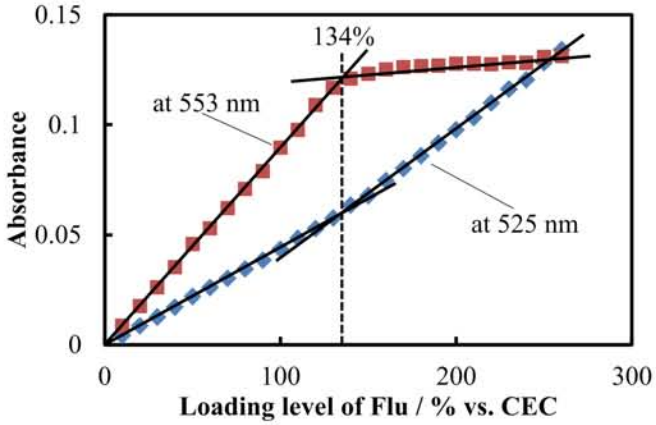


Figure 3-5. Lambert-Beer plots of Fluorone/clay complexes at 553 nm(■) and 525 nm(◆) in water.

We have found out that tetra cationic porphyrin adsorb on the clay surface without aggregation below 100% adsorption vs. CEC due to Size Matching Effect. In the case of Fluorone, the maximum adsorption ratio is 134% vs. CEC (0.27 molecules $nm^{-2}$) of the clay. To explain why Fluorone can adsorb on the clay surface up to 134% vs. CEC, the adsorption behavior of Fluorone on the clay surface is discussed below. At 134% vs. CEC adsorption condition, one Fluorone molecule, which has four cationic sites, should occupy three anions on the clay surface. This indicates that Fluorone has one excess cationic site, which is not neutralized by anionic charge of the clay. The excess cationic part of Fluorone may have a counter anion, which should be iodide ion in this case. To confirm whether iodide ion exists or not, the Fluorone/clay complex film was prepared with filtration and was measured by X-ray fluorescence (XRF) spectrometer. Amount of iodide anion in the sample before filtration is 0.10 mmol $L^{-1}$. During the preparation procedure of membrane, iodide anions, which do not adsorb on

this film as a counter ion, should be removed. As a result, the iodide anions were not detected in Fluorone/clay film as shown in Figure 3-6.

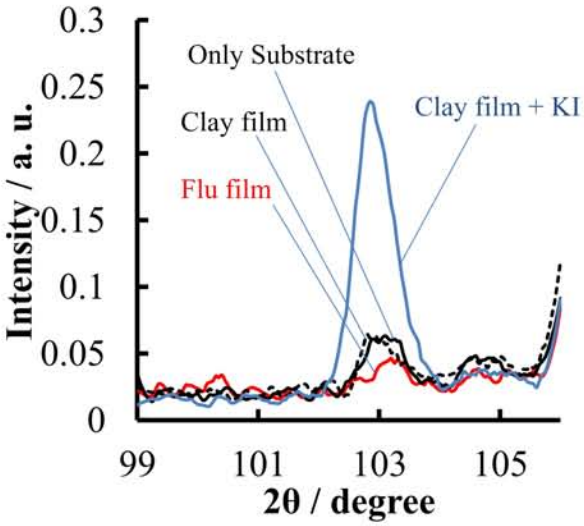


Figure 3-6. XRF spectra of the Fluorone/clay complex film (red line), the clay film with KI ($5.0 \times 10^{-8}$ mol) (blue line), the clay film (broken line) and the glass substrate (black line) under vacuum.

This result indicates that excess cationic charge in Fluorone is neutralized not by counter iodide ion but by an anionic part in the adjacent Fluorone molecule, that is, there is an electrostatic attractive interaction between adjacent Fluorone molecules. Supposing that Fluorone is tri-cationic molecule which has 4 cationic charges and 1 anionic charge, the electrostatic interactions between charges of Fluorone and anions on the clay was estimated based on the calculation of Self-Consistent Field (SCF) method. At first, adsorption orientation of a single Fluorone molecule on the clay surface was determined. The adsorption structure of Fluorone on the clay surface was discussed by estimating a total coulombic interaction. The coulombic force F (in N) is expressed as eq 3-1.

$$F = \frac{q_1 q_2 N_A}{4\pi\varepsilon_0 \varepsilon r^2} \qquad \text{eq 3-1}$$

where $q_1$ and $q_2$ are the electrical charge of matter$_1$ and matter$_2$, respectively, $N_A$ is the Avogadro constant, $\varepsilon$ is the relative dielectric constant, $\varepsilon_0$ is the dielectric constant under vacuum ($8.85 \times 10^{-12}$ C$^2$ J$^{-1}$ m$^{-1}$), and $r$ is the distance between matter$_1$ and matter$_2$ (in m). To determine the adsorption structure of

Fluorone on the clay surface, the F values between Fluorone and clay are calculated as follows. In this calculation, the charges in Fluorone molecules and clay surface are defined to be localized in the center of N atom in 2, 4, 5, 7-substituent, O atom in 3, 6-substituent and the center of Al atom of clay, respectively. It was supposed that the charge of N atom in 2, 4, 5, 7-substituent was +1, the charge of O atom in 3, 6-substituent was -0.5 (× 2) and the charge of Al atom of clay was -1, respectively. The intercationic site distances in Fluorone molecules were calculated by DFT method. DFT calculations were performed at the B3LYP/6-31G* level, as shown in Figure 3-7 (a). In the present system, the average interanionic site distance on the clay surface is 1.2 nm on the basis of a hexagonal array. To determine the r values, the distance of the vertical direction to Al atom below the clay surface from Fluorone ring (3.7 Å) was determined by the half of the 2, 4, 5, 7-substituents's width (3.4 Å) and the distance from the center of Al atom to the surface of O atoms surrounding Al atom (0.3 Å). Using these parameters, the r value, when |F| was maximum, was calculated by Self-Consistent Field (SCF) method and the most stable adsorption orientation of Fluorone molecule on the clay surface as shown in Figure 3-7 (a) were determined.

Next, adsorption assembly structures of Fluorone molecules on the clay surface were determined. Using the structure of the most stable adsorption orientation of Fluorone molecule on the clay surface, the adsorption structure of Fluorone on the clay surface at the high dye loading was proposed as shown in Figure 3-8 on the basis of hexagonal array. In these figures, Fluorone molecules were expressed in van der Waars' radius. These figures were proposed on the basis of some conditions (1; The steady contact with each Fluorone molecules such as aggregation with π-π stacking did not occur. 2; The Used adsorption structure was only the structure such as shown in Figure 3-7 (a) which was the most stable adsorption orientation of Fluorone molecule on the clay surface. 3; All anions on the clay surface were neutralized by cations of Fluorone.). Figure 8 did not determine the actual orientation of adsorbed Fluorone molecules and there were the different orientations from these figures. Figure 3-7 (b) and Figure 3-8 were described Fluorone's adsorption density (0.27 molecules $nm^{-2}$) on the clay surface. As

a result of that counter anions ($I^-$) for remained cations of adsorbed Fluorone were not observed by XRF measuring, it was supposed that those remained cations were neutralized by coulombic interaction between inter-Fluorones. Based on this supposition, the adsorption structures of two Fluorone molecules as shown in Figure 3-9 were proposed. Figure 3-9 (a) and (b) were the adsorption structure which the distance between a remained cation part of one Fluorone and the anion part of another Fluorone was shortest. Such structures have the advantage of the neutralization by inter-molecules interaction. Using only the adsorption structure as shown in Figure 3-7 (a), Fluorone could not be arranged in hexagonal array. Then, the adsorption structure as shown in Figure 3-7 (b) was estimated the reasonable structure which was considered coulombic interactions and adsorption density, and the adsorption structure as shown in Figure 3-7 (b) was selected as the proposed structure.

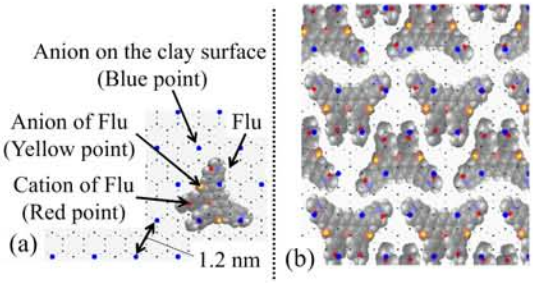


Figure 3-7. Proposed adsorption structure of Fluorone on the clay surface. (a) The most stable structure that affords the maximum electrostatic interaction between Fluorone and clay. (b) The adsorption structure of Fluorone on the clay surface at 134% adsorption vs. CEC.

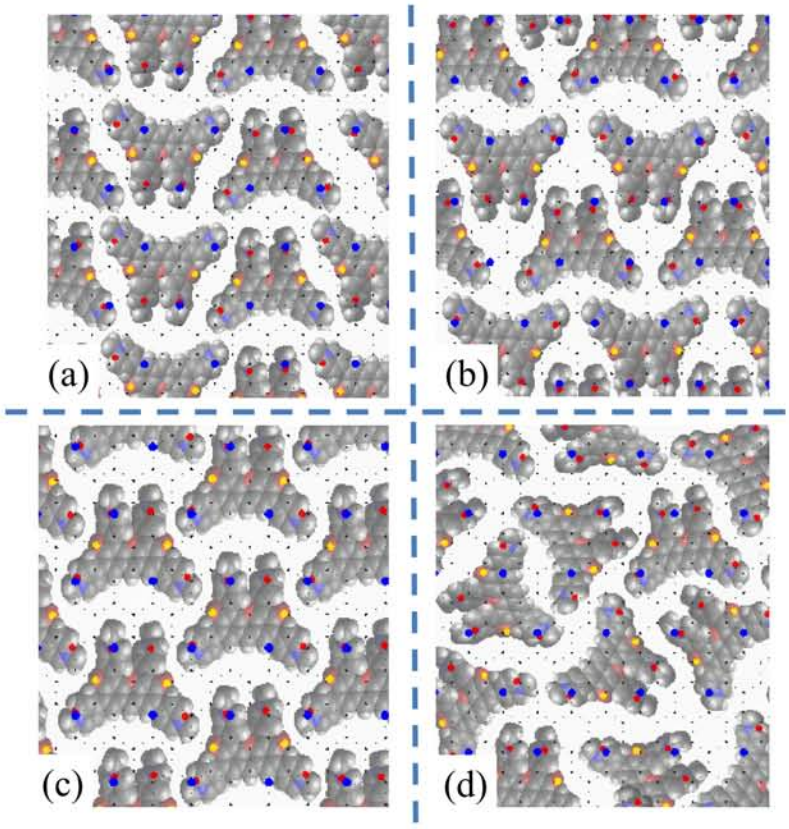


Figure 3-8. Proposed adsorption structure of Fluorone on the clay surface. (a) Fluorone are arranged in rows, (b) Fluorone are arranged in staggered rows, (c) all Fluorone molecules are same orientation and (d) a random adsorption structure.

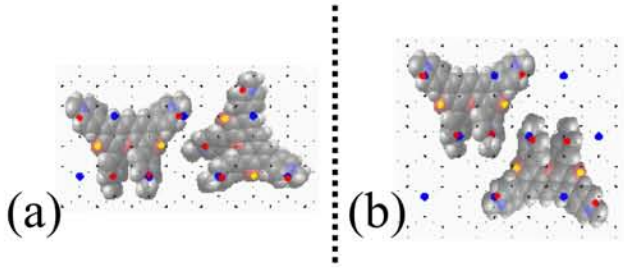


Figure 3-9. Proposed adsorption structure of Fluorone on the clay surface. (a) and (b) were the proposed structures of two Fluorone molecules on the clay surface.

As a result, the most stable adsorption orientation of Fluorone molecule on the clay surface was determined as shown in Figure 3-7 (a). This adsorption orientation affords the maximum electrostatic interaction energy between charges of Fluorone and clay. In this figure, Fluorone was expressed using van der Waars' radius. Using the structure of Figure 3-7 (a), the adsorption structure of Fluorone on the clay surface at the high dye loading (134% vs. CEC) was proposed as shown in Figure 3-7 (b) on the basis of hexagonal array. The other patterns of possible adsorption structure of Fluorone are shown in Figure 3-8. Among them, the adsorption structure shown in Figure 3-7 (b) would be the most possible one, judging from the electrostatic neighboring of cationic part of Fluorone and anionic part of adjacent Fluorone and the steric condition.

Thus, I concluded that the cooperation of an electrostatic attractive interaction between Fluorone molecules and between Fluorone and clay, that is Size-Matching Effect, leads to the high density adsorption of Fluorone without aggregation on the clay surface.

- ***Fluorescence behavior of Fluorone with and without clay in water***

Fluorescence spectra of Fluorone with and without clay in water are shown in Figure 3-10. The loading level of Fluorone was 0.025, 0.06, 5 and 40% vs. CEC of the clay. The $\lambda_{max}$ of fluorescence spectra were shifted from 565 nm to 580 nm upon adsorption on the clay surface as in the case with absorption. While the fluorescence quantum yield ($\phi_f$) of Fluorone without clay was 0.52, $\phi_f$ with clay was 0.50, when the loading level of Fluorone is low (0.025 and 0.06% vs. CEC). The excimer emission was not observed at any loadings. As the loading level of Fluorone increased from 0.06% to 40% vs. CEC as shown in Figure 3-11, the fluorescence intensity decreased. Because all absorption spectra of these samples completely coincide (not shown), this fluorescence quenching phenomenon is not due to a static process, but due to a dynamic one. This self-fluorescence quenching would be due to an electron transfer from excited Fluorone to adjacent Fluorone. It should be noted that relatively high $\phi_f$ (0.10) was obtained even at 40% adsorption density vs. CEC that corresponds to 0.080 molecules $nm^{-2}$, without

any diluting reagent. In the case of reported fluorescent system such as rhodamine/clay complex, the adsorption density of rhodamine was not so high (0.00094~0.0031 molecules $nm^{-2}$) because of the dilution with surfactant to suppress the aggregation of rhodamine dye.[44, 45]

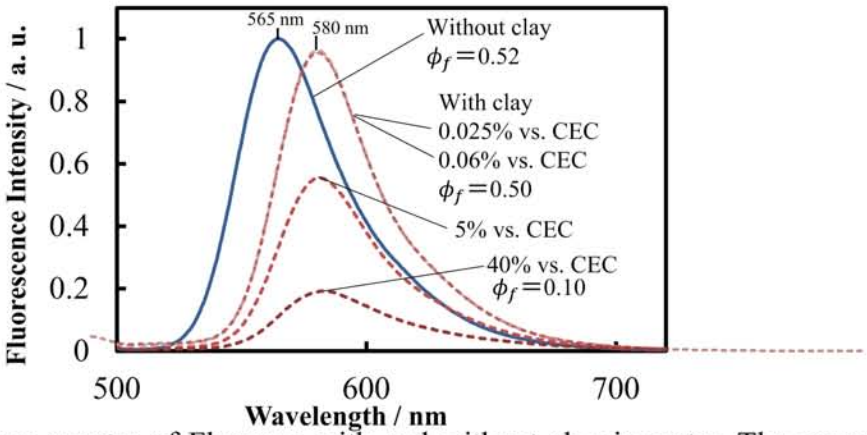


Figure 3-10. Fluorescence spectra of Fluorone with and without clay in water. The concentration of Fluorone was $1.0 \times 10^{-7}$ mol $L^{-1}$ for all samples. The concentrations of clay were 160, 67, 0.80 and 0.10 mg $L^{-1}$, and the loading levels are 0.025, 0.06, 5 and 40% vs. CEC, respectively. A 430 nm long pass filter was set in front of detector. The excitation wavelength was 420 nm. Fluorescence quantum yield ($\phi_f$) values were determined using rhodamine 6G ($\phi_f$ = 0.95) as a standard in aerated condition.[26]

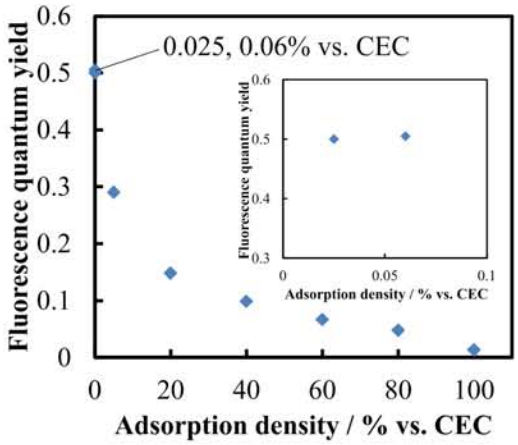


Figure 3-11. Fluorescence quantum yields ($\phi_f$) of Fluorone/clay complexes at various clay concentrations in water. The concentration of Fluorone was $1.0 \times 10^{-7}$ M. Inset: 0 - 0.1% vs. CEC. A 430 nm long pass filter was set in front of detector. The excitation wavelength was 420 nm. Fluorescence quantum yield ($\phi_f$) values were determined using rhodamine 6G ($\phi_f = 0.95$) as a standard in aerated condition.[47]

• ***The time-resolved fluorescence measurements for Fluorone/clay complex***

The time-resolved fluorescence spectra were measured for Fluorone and Fluorone/clay complex by using the picoseconds fluorescence measurement system. The fluorescence decay curves for Fluorone with and without clay excited at 406 nm are shown in Figure 3-12. For the sample with clay, the dye loading was set at 0.06% vs. CEC of the clay. As can be seen, both the decay curves for Fluorone and Fluorone/clay complex can be analyzed as a single exponential decay, and the excited lifetimes ($\tau_s$) were determined to be 2.8 ns and 2.9 ns, respectively.

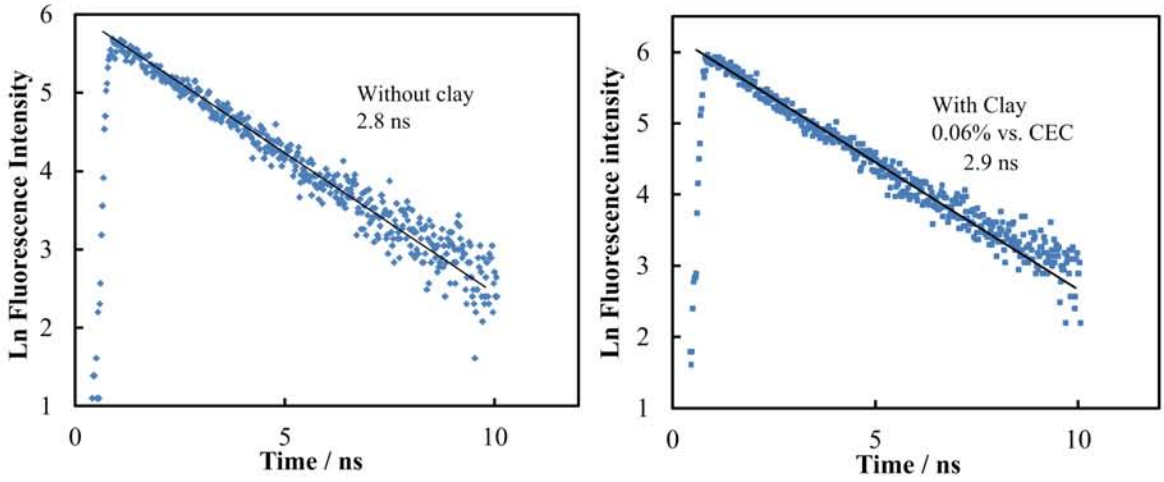


Figure 3-12. The fluorescence decay of Fluorone (left) and Fluorone/clay complex (right) at 0.06% dyes loadings in water ([Fluorone] = $1.0 \times 10^{-6}$ M). The excitation wavelength was 406 nm (FWHM = 71 ps). Monitored wavelengths were 565 nm (without clay) and 580 nm (with clay).

According to the values of $\phi_f$ (0.50) and $\tau_s$ (2.9 ns) of adsorbed Fluorone on the clay surface, nonradiative deactivation rate constant ($k_d$; $k_d = (1 - \phi_f) / \tau_s$) and radiative deactivation rate constant ($k_r$; $k_r = \phi_f / \tau_s$) is calculated to be $1.7 \times 10^8$ $s^{-1}$ and $1.7 \times 10^8$ $s^{-1}$, respectively. These results indicate that the photochemical property of Fluorone is intrinsically kept on the clay surface at low loading levels. The excited lifetime of Fluorone on the clay surface was long enough to undergo photochemical reactions such as excited energy transfer. We believe that this complex is useful for constructing the system of photochemical reactions.

### 3-1-4. Conclusion

In the present paper, the novel tetra cationic xanthene derivative (Fluorone) was synthesized and its photochemical behaviors with and without clay were investigated. Fluorone adsorbed on the clay surface up to 134% vs. CEC without an aggregation. The maximum adsorption density of Fluorone on the clay surface was calculated to be 0.27 molecules $nm^{-2}$. We concluded that interaction between adjacent Fluorone molecules and Size-Matching Effect leads to such high density adsorption without aggregation. It is found out that fluorescence properties such as $\phi_f$ and $\tau_s$ are intrinsically retained upon complex formation with clay. Although the fluorescence intensity decreased with increasing the dye loadings, $\phi_f$ value (0.10) was enough high even at high density condition (0.080 molecules $nm^{-2}$) without any diluting reagent.

## 3-2. 1,3,6,8-*tetrakis*(*N*-methylpyridinium-3-yl)pyrene tetrachloride (Pyrene)

### 3-2-1. Introduction

Pyrene derivatives have a high fluorescence quantum yield and an enough long fluorescence lifetime as photo-functional dyes. Although fluorescent pyrene-clay complex has been investigated. In this study, we designed and synthesized the tetra cationic pyrene dye (Pyrene: Figure 3-13) and investigated its adsorption and photochemical behavior with and without clay in water.

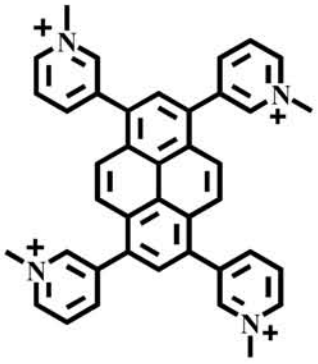

Figure 3-13. 1,3,6,8-*tetrakis*(*N*-methylpyridinium-3-yl)pyrene tetrachloride (Pyrene)

### 3-2-2. Experimental Section

1,3,6,8-*tetrakis*(*N*-methylpyridinium-3-yl)pyrene tetrachloride ($Pyrene^{4+}$) was synthesized as shown in Figure 3-14.

・***Synthesis of 1,3,6,8-tetrakis(pyridin-3-yl)pyrene***

*1,3,6,8-tetra*bromopyrene (131 mg), 3-(boronic acid) pyridine (167 mg) and pottasium carbonic acid (179 mg) were added to degassed DMF (100 mL) under $N_2$. After tetrakis（triphenylphosphine）palladium (10 mg) was added to the mixture, it was heated to 120°C for 3 days. 40 hours later, 3-(boronic acid) pyridine (118 mg) and tetrakis（triphenylphosphine）palladium (30 mg) were added. After cooling, the reaction solution was added into acetone (1.5 L) and the black solid (141 mg) was obtained with filtration (PTFE membrane filter (pore size: 0.1 μm)). Then, it was dissolved in mixed

solvent (dichloromethane : acetonitrile = 1 : 2 (v : v)) and the solution was heated at 50 °C for 3 hours. After cooling, the solution was cooled at 5 °C for 8 hours, and the dilute yellow solid (80 mg: Yield 62%) was added with filtration (PTFE membrane filter (pore size: 0.1 μm)). $^1$H-NMR: (CDCl, 500 MHz) δ: 8.96(d, 4H, 2.16 Hz), 8.78-8.80(m, 4H), 8.19(s, 4H), 8.05(s, 2H), 8.02-8.04(m, 4H), 7.54-7.56(m, 4H) ppm.

- ***1,3,6,8-tetrakis(N-methylpyridinium-3-yl)pyrene tetrachloride (Pyrene$^{4+}$)***

Synthesized 1,3,6,8-tetrakis(pyridin-3-yl)pyrene (30 mg) was dissolved in degassed DMSO (5 mL), and iodomethane (1 mL) was added to the solution. The mixture was stirred for 4 hours at 40°C. After cooling, the solution was slowly added into 1 L dichloromethane. The precipitates were collected by filtration (PTFE, 0.1 μm, Millipore) and were dispersed into acetone. Then, the precipitates were collected by filtration (PTFE, 0.1 μm, Millipore). The counter ion (iodide) was exchanged to chloride ion by the use of the ion exchange resin. The solvent was removed by evaporation and the obtained solid was heated to 60°C in vacuum for 4 hours. The yellow solid was obtained (30 mg, Yield 71%). $^1$H-NMR: ($D_2O$, 500 MHz) δ: 9.17(s, 4H), 8.93(d, 4H, 6.47 Hz), 8.82(d, 4H, 8.32 Hz), 8.22-825(m, 4H), 8.21(s, 2H), 8.20(s, 4H), 4.48(s, 12H) ppm.

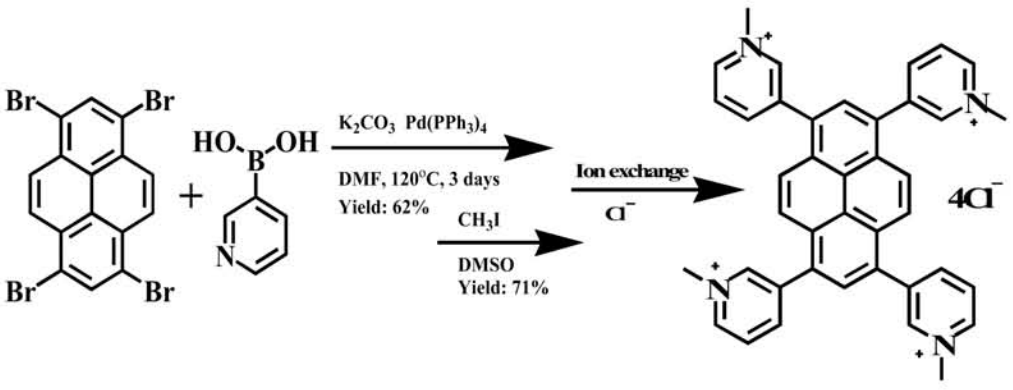


Figure 3-14. The synthesis scheme of 1,3,6,8-*tetrakis*(*N*-methylpyridinium-3-yl)pyrene tetrachloride (Pyrene$^{4+}$).

### 3-2-3. Result and Discussion

**・Adsorption Behavior**

Adsorption behavior was evaluated by the absorption spectrum. Absorption spectra of Pyrene with and without clay were shown in left of Figure 3-15. The absorption maxima are 412 and 386 nm, respectively. Then the red shift of 26 nm was observed by adsorption on clay surface. This behavior can be rationalized by the planarization of the molecular structure on the clay surface as shown in Figure right of 3-15. Whereas pyridinium ring of Pyrene is almost vertical to pyrene ring in the water, pyridinium ring can be co-planarized with adsorption on the clay. This planarization expanded a conjugated system of the pyrene ring and caused red shift of the absorption maximum.

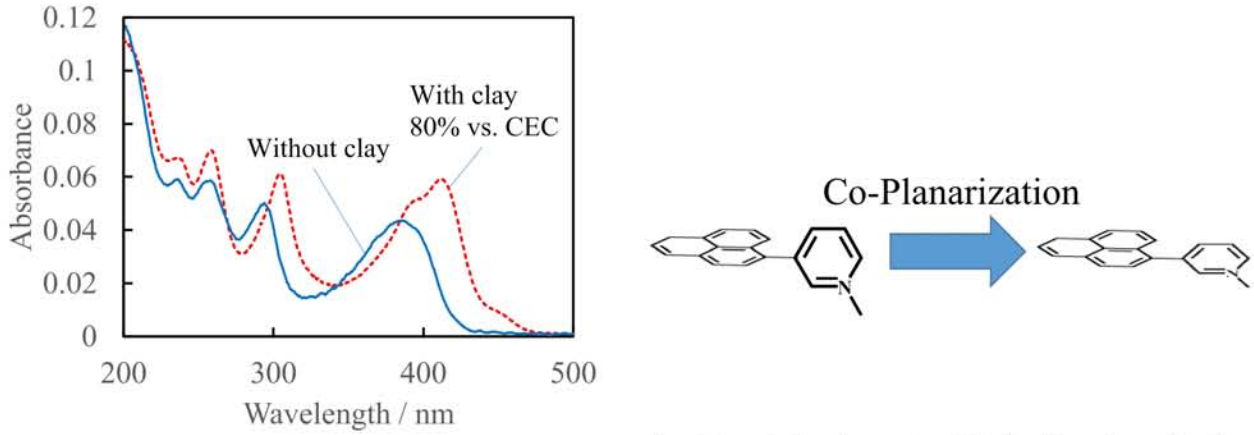


Figure 3-15. Left: Absorption spectra of Pyrene with and without clay in water. Right: Co-planarization

In order to explain the spectral red shift by co-planarization, the molecular structures were optimized by DFT method (B3LYP/6-31G(d, p)), and the excitation energies were calculated by TD-DFT method (B3LYP/6-31G(d, p)). The condition without clay was calculated without any structure fixation, and the condition with clay was calculated with assuming that the dihedral angle between the pyridinium ring and pyrene ring was immobilized at 45 degree. Calculation results were shown in Figure 3-16. The vertical axis of bottom Figure 3-16 shows the excitation energy, and red line indicates allowed transition, black or blue line indicates a forbidden transition. This allowed transition without clay was a higher energy state than this forbidden transition. This allowed transition indicated the HOMO-LUMO

transition, and the HOMO-LUMO transition with clay was a low-energy transition than the forbidden transition as shown in Figure 3-16. Whereas the HOMO was not much change before and after the rotation of the dihedral angle, LUMO was stabilized by expansion of conjugated system. The difference of the transition energy was calculated to be 0.314 eV. And then, the actual energy difference before and after adsorption on clay was calculated to be 0.203 eV. Judging from these energy values, absorption spectra of $Pyrene^{4+}$/clay complex could show red shift due to co-planarization of pyridinium rings.

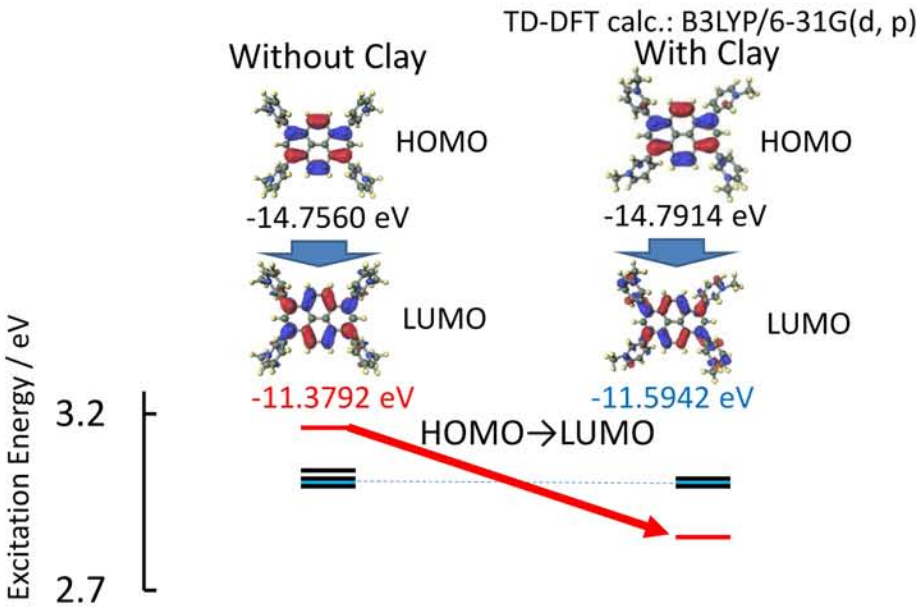


Figure 3-16. Calculation results of Pyrene structure and excitation energy. The vertical axis of bottom shows the excitation energy, and red line indicates allowed transition, black or blue line indicates a forbidden transition.

Absorption spectra at various Pyrene loadings vs. clay nano-sheet were shown in Figure 3-17. The dye loadings were changed by adjusting the concentration of Pyrene. The concentration of clay was always kept constant at 8.0 mg $L^{-1}$. While the spectra retained same shape below 80% vs. CEC adsorption, the observed spectral shape changed above 90%. The $\lambda_{max}$ (386 nm) and the spectral shape of new species above 90% are same as that of $Pyrene^{4+}$ in water without clay. All spectra can be expressed by the combination of the component of the adsorbed $Pyrene^{4+}$ on the clay surface and it of

non-adsorbed Pyrene. The Lambert-Beer plot for Pyrene/clay complexes at 412 nm is shown in right of Figure 3-17. As shown in Figure 3-17, the linearity of the plot was observed below 85% vs. CEC of the clay. Thus, it turns out that the Pyrene does not form aggregate in the ground sate and exists as a single molecule for 0-85% vs. CEC.

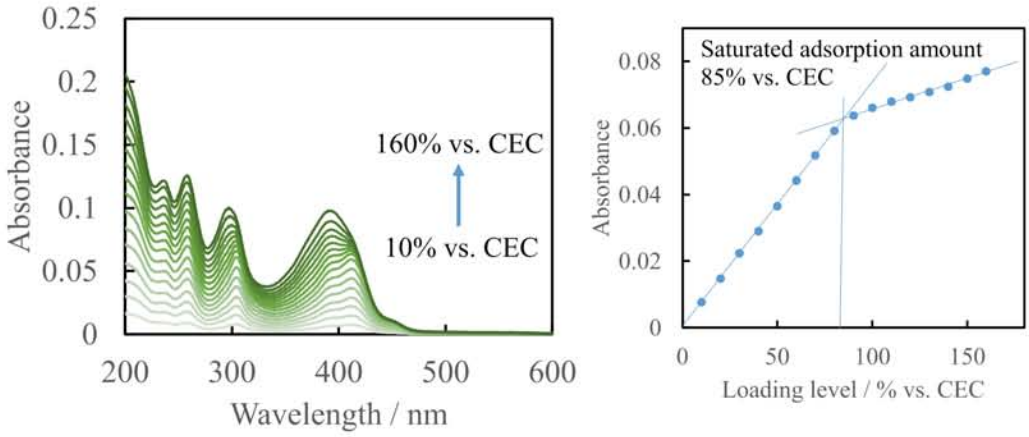


Figure 3-17. Left: Absorption spectra of Pyrene with clay in water. Right: Absorbance of Pyrene with clay in water at 412 nm.

・**Fluorescence Behavior**

Fluorescence spectra of Pyrene showed red shift of 23 nm by adsorption onto the clay surface as shown in Figure 3-18. This red shift was caused by the co-planarization in a similar way to absorption behavior. Furthermore, the fluorescence quantum yield of Pyrene with and without clay was 0.36 and 0.03, respectively, and the fluorescence quantum yield with absorption onto the clay surface was about 12 times. In order to discuss this behavior in more detail, the time-resolved fluorescence was measured.

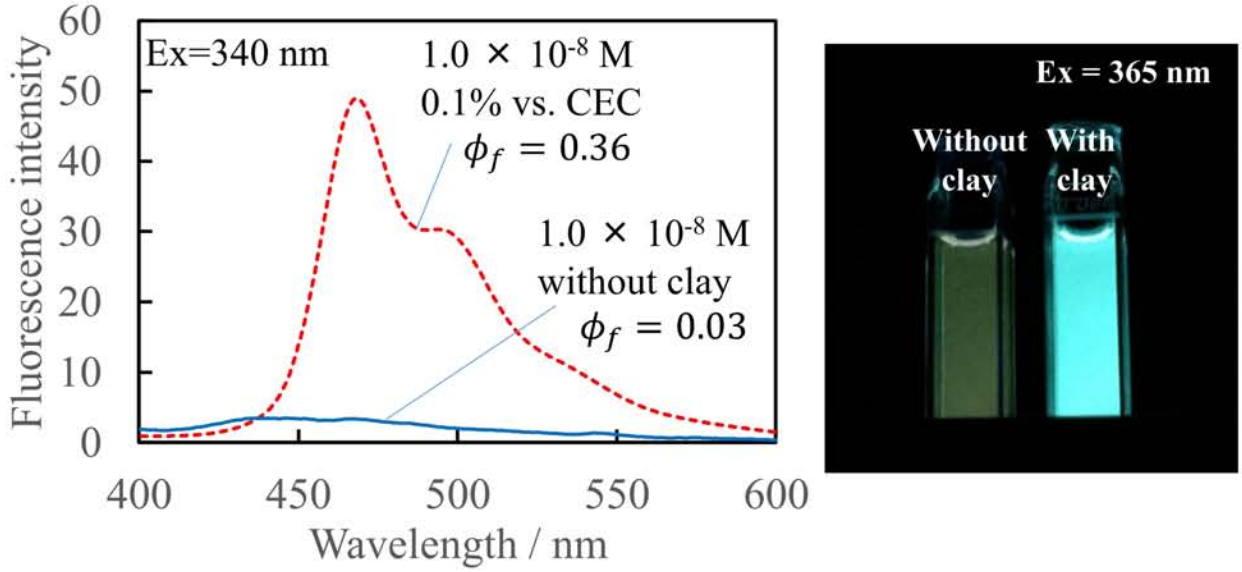


Figure 3-18. Fluorescence spectra of Pyrene with and without clay in water

As a result, the excited lifetimes with and without clay can be fitted with single-component, and these were 2.8 and 2.9 ns, respectively as shown in Figure 3-19.

$$\boldsymbol{\phi_f = \frac{k_f}{k_{vib}+k_{isc}+k_f} = k_f\,\tau_f} \quad \cdot\cdot\cdot \textbf{(eq. 3-2)}$$

By using these results and eq. (3-2), photophysical parameters were calculated as shown in Table 3-1. Obtained radiative rate constants and non-radiative deactivation rate constants were compared. Then, the radiative rate constant was about 13 times increased with clay, and non-radiative deactivation rate constant decreased about 70% with clay. Judging from these results, the relative fluorescence enhancement was mainly induced by the increase of radiative deactivation.

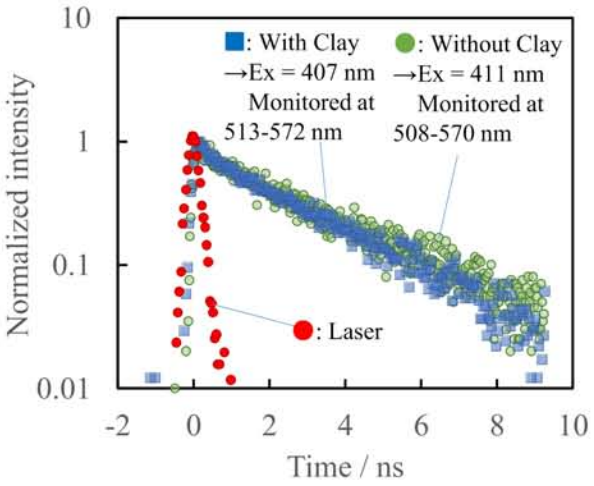


Figure 3-19. Fluorescence decays of Pyrene and Pyrene / clay complex at 0.1% vs. CEC in water ([Pyrene] = $0.1\times10^{-7}$ M). Excitation wavelengths were 407 nm (with clay) and 411 nm (without clay). Monitored wavelengths were 513-572 nm (with clay) and 508-570 nm (without clay).

Table 3-1. Photophysical parameter of Pyrene with and without clay in water

| | $\tau_f$ / ns | $\phi_f$ | $k_f$ / $10^7$ $s^{-1}$ | $k_{nr}$ / $10^8$ $s^{-1}$ |
|---|---|---|---|---|
| With clay | 2.8 | ↑ 0.36 | ↑ 13 | ↓ 2.3 |
| Without clay | 2.9 | 0.03 | 1.0 | 3.3 |

If this order of transition energy does not change at the excited state, the mechanism of luminescence enhancement can be explained. As discussed previously, dihedral angles are rotated by adsorbed on the clay surface, and a conjugated system is expanded. Thereby it is supposed that the reversal of allowed transition and forbidden transition is occurred as shown in Figure 3-16.

As a result, I supposed that the radiation rate constant and fluorescence quantum yield were increased due to such a change of energy level changes by the effect of complex formation with clay.

### 3-2-4. Conclusion

Tetra cationic pyrene derivative (Pyrene) was synthesized successfully. The luminescence behavior of Pyrene on the clay surface was investigated and the fluorescence quantum yield increased. The fluorescence quantum yield of Pyrene increased about 12 times by adsorption on the clay surface (0.03→0.36). Judging from the result of lifetime measurement, it was found that the fluorescence rate constant was increased. It is considered that this increase of the fluorescence rate constant is due to the fact that the first excited state, which was forbidden, became an allowed transition by adsorption on the clay surface.

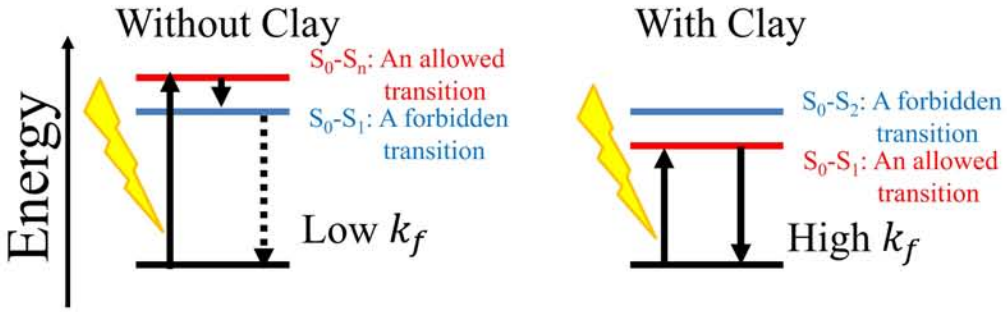

# 4. Efficient Energy Transfer Reaction

Among those researches including ours, authors noticed that there is no standard way to express the performance of artificial LHS. One of the typical values to evaluate the performance of artificial LHS is enhancement ratio of photochemical reaction by applying the LHS when monochromatic excitation light at specific wavelength is used. In this method, the different enhancement ratio will be observed by the change of excitation wavelength. For example, if the excitation wavelength where energy acceptor does not absorb is used, the enhancement ratio could be infinite theoretically. On the other hand, the number of energy donor molecule which transfers the excited energy to one energy acceptor molecule have been measured in order to evaluate the ability of LHS. In the traditional method, the enhancement ratio of the excitation frequency cannot be estimated. Therefore, we propose the newly defined parameter, the enhancement ratio of the excitation frequency of the energy acceptor, in order to estimate the performance of LHS universally.

In this section, energy transfer among three dyes (Fluorone, *m*-TMPyP and *p*-TMPyP) was studied to utilize more wide range of visible light leading to an increase of the excitation frequency of *p*-TMPyP that is the final energy acceptor in the system. Structures of Fluorone, *m*-TMPyP and *p*-TMPyP are shown in Figure 4-1. The order of excitation energies of these three dyes is Fluorone > *m*-TMPyP > *p*-TMPyP. Thus, the excited energy was transferred from Fluorone and *m*-TMPyP to *p*-TMPyP.

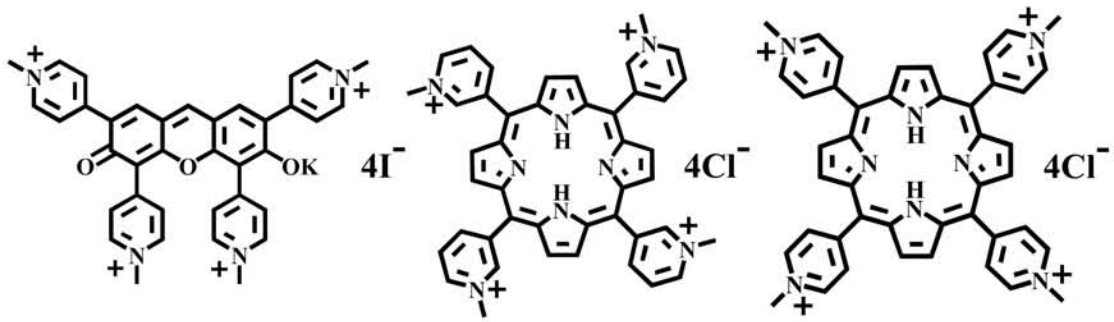

Figure 4-1. The structures of *p*-2,4,5,7-tetrakis(*N*-methylpyridinium-4-yl)-6-pottasiumoxy-3-fluorone tetraiodide (Fluorone; left), *meso*-tetra (*N*-methyl-3-pyridyl) porphine tetrachloride (*m*-TMPyP; center) and *meso*-tetrakis(*N*-methylpyridinium-4-yl) porphyrin tetrachloride (*p*-TMPyP; right).

# 4-1. Energy Transfer Reaction between Two Components

## 4-1-1. Introduction

At first, I investigated energy transfer reaction between two dyes toward an energy transfer reaction among three components. The energy transfer reaction between *m*-TMPyP and *p*-TMPyP has already been investigated by our research group.[31]

## 4-1-2. Experimental Section

・***Materials***

*p*-2,4,5,7-tetrakis(*N*-methylpyridinium-4-yl)-6-pottasiumoxy-3-fluorone tetraiodide (Fluorone) was synthesized by the method which was described in the previous section.

・***Preparation methods for the clay/dye complexes***

Typical procedure to prepare energy transfer samples was as follows. In this experiment, Fluorone, *m*-TMPyP, and *p*-TMPyP were used as cationic dyes. Aqueous solutions of different two kind of dyes were mixed. The obtained solutions were mixed with an aqueous clay solution (9.9 mg $L^{-1}$) under vigorous stirring. The total concentrations of dyes were set at $1.0 \times 10^{-7}$ M, and the clay loadings were changed by changing the concentration of clay. Under these conditions, the clay sheets exist in a form of individually exfoliated sheets and the obtained solution was substantially transparent.

・***Theoretical Energy Transfer Rate Constant***

We suppose that the mechanism of energy transfer reaction is Förster type[48] in this system. Before the experiment, we calculated the theoretical energy transfer rate constant $k_{ET}$ using Förster eq. (4-1),

$$k_{ET} = \frac{9000 \ln 10 \kappa^2 \phi_D}{128\pi^5 n^4 N \tau_D R^6} J, \qquad (4\text{-}1)$$

, where $\kappa$ is the orientation parameter ($\kappa^2$ = 5/4 for in-plane orientation), $\phi_D$ is the fluorescence quantum yield of energy donor (The fluorescence quantum yields of Fluorone, *m*-TMPyP and *p*-TMPyP were 0.50, 0.081 and 0.048, respectively), $n$ is the refractive index of the bulk medium ($n$ = 1.33 in the case of water), $N$ is the Avogadro constant, $\tau_D$ is the excited singlet lifetime of donor on the clay surface (the excited singlet lifetime of Fluorone, *m*-TMPyP and *p*-TMPyP were 2.9, 8.9 and 5.6 ns, respectively), $R$ is the center-to-center distance between adsorbed dyes (2.4 nm under 100% vs. CEC condition; this value is the average distance between molecules), and $J$ is the spectral overlap integral between the fluorescence spectrum of donor and the absorption of acceptor according to equation (4-2).

According to the analysis of the overlap between the fluorescence of the donor molecule and the absorption of the acceptor, based on equation (4-2), the spectral overlap integral $J$ for each combination were calculated.

$$J = \sum F_D(\lambda) \varepsilon_A(\lambda) \lambda^4 \Delta\lambda, \qquad (4\text{-}2)$$

, where $\lambda$ is the wavelength in cm, $\varepsilon_A(\lambda)$ is the extinction coefficient of the acceptor at wavelength $\lambda$ and $F_D(\lambda)$ is the fraction of the total fluorescence intensity of donor. $J$ and $k_{ET}$ for each combination in

this system were calculated and shown in Table 4-1. Deactivation rate constants (= 1 / τ) of energy donor such as Fluorone was calculated to $3.4 \times 10^8$ $s^{-1}$, respectively. The $k_{ET}$ values are larger than this deactivation rate constant. Therefore, judging from $k_{ET}$ values, most of the excited energy should transfer to *m*-TMPyP and *p*-TMPyP from Fluorone efficiently.

Table 4-1. Calculated *J* Values and $k_{ET}$ of Each Energy Transfer Reaction

| Donor→Acceptor | J / $10^{-14}$ $M^{-1}$ $cm^{-1}$ $cm^4$ | $k_{ET}$ / $10^9$ $s^{-1}$ |
|---|---|---|
| Fluorone→*m*-TMPyP | 4.4 | 14 |
| Fluorone→*p*-TMPyP | 16 | 50 |
| *m*-TMPyP→*p*-TMPyP | 1.8 | 0.30 |

### 4-1-3. Results and Discussion

• ***Energy Transfer Reaction between Fluorone and p-TMPyP***

At first, the absorption spectrum of Fluorone/*p*-TMPyP/clay complex, where their loading levels are 20%, was measured, and it was found out that the spectrum was completely identical with a sum of individual absorption spectra of Fluorone/clay and *p*-TMPyP/clay complexes as shown in Figure 4-2. Thus, it was found out that an aggregation is completely suppressed and the dye molecules exist as a single molecule, when two types of dye co-exist on the clay surface.

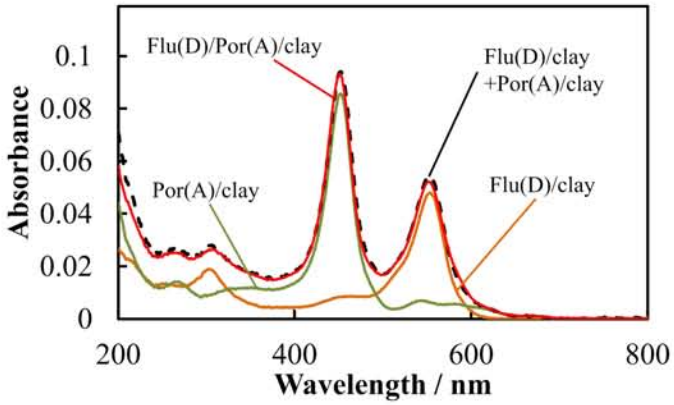


Figure 4-2. Absorption spectra of Fluorone/clay ([Fluorone] = $5.0\times10^{-7}$ M, 20% vs. CEC), *p*-TMPyP/clay ([*p*-TMPyP] = $5.0\times10^{-7}$ M, 20% vs. CEC), a sum of individual absorption spectra of them and co-adsorption sample ([Fluorone] = $5.0\times10^{-7}$ M, [*p*-TMPyP] = $5.0\times10^{-7}$ M, 20% vs. CEC)

The energy transfer from the excited singlet state of Fluorone to the ground state of *p*-TMPyP on the clay surface was examined by measuring steady-state fluorescence spectra. Individual fluorescence spectra of Fluorone/clay and *p*-TMPyP/clay complexes and energy transfer sample of Fluorone/*p*-TMPyP/clay complex are shown in Figure 4-3. The dye loadings of 0.06% vs. CEC for individuals

and 100% vs. CEC for Fluorone/*p*-TMPyP/clay complex were set at $5.0 \times 10^{-8}$ M, respectively. The mol ratio of Fluorone to *p*-TMPyP was 1 to 1 for all Fluorone/*p*-TMPyP/clay complex. The excitation wavelength was set 510 nm. The fluorescence spectral shape of energy transfer sample showed that the intensity of acceptor fluorescence increased and the donor fluorescence was quenched.

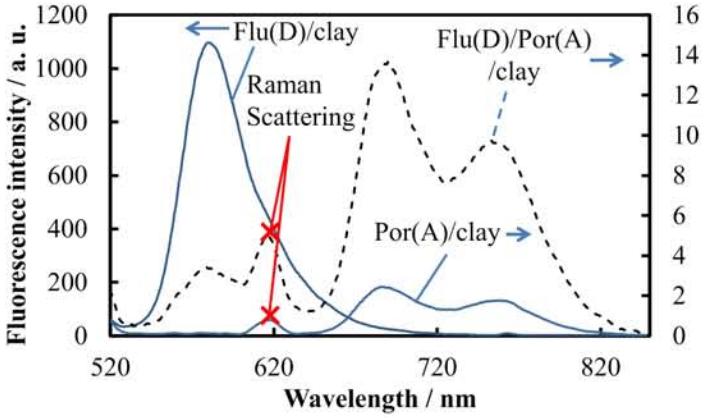


Figure 4-3. Fluorescence spectra of Fluorone/clay ([Fluorone] = $5.0 \times 10^{-8}$ M; 0.06% loadings), *p*-TMPyP/clay ([*p*-TMPyP]= $5.0 \times 10^{-8}$ M; 20% loadings) and Fluorone/*p*-TMPyP/clay ([Fluorone] = [*p*-TMPyP] = $5.0 \times 10^{-8}$ M;100% loadings) complexes in water. The excitation wavelength was 510 nm. The intensity of Fluorone/clay fluorescence was indicated on the left vertical axis, and those of Fluorone/*p*-TMPyP/clay and *p*-TMPyP/clay fluorescence were indicated on the right vertical axis.

By using the fluorescence spectra of Fluorone, *p*-TMPyP and Fluorone/*p*-TMPyP/clay complexes, the energy transfer efficiency ($\eta_{ET}$) and the self-quenching efficiency of donor ($\phi_{qD}$) can be calculated as follows.

The total fluorescence of energy transfer sample (Fluorone/*p*-TMPyP/clay complex) ($F_{ET}(\nu)$) can be expressed by equation (4-3).

$$F_{ET}(\nu) = \left(1 - \eta_{ET} - \phi_{qD}\right)F_D^0(\nu) + \left\{1 + \frac{\left(1-10^{-A_D}\right)}{\left(1-10^{-A_A}\right)}\eta_{ET}\right\}F_A^0(\nu), \qquad (4\text{-}3)$$

where $F_{ET}(\nu)$ is the fluorescence spectrum of energy transfer sample (Fluorone/*p*-TMPyP/clay complex), $F_D^0(\nu)$ is that of energy donor (Fluorone/clay complex), $F_A^0(\nu)$ is that of energy acceptor (*p*-TMPyP/clay complex), $A_D$ and $A_A$ are absorbance of energy donor and energy acceptor at excitation wavelength (510 nm), respectively, $\eta_{ET}$ is the energy transfer efficiency, defined in equation (4-4), $\phi_{qD}$ is the quenching efficiency due to an electron transfer and/or an enhanced thermal deactivation process due to the collision between neighboring guests, defined in equation (4-5).

$$\eta_{ET} = \frac{k_{ET}}{k_{ET}+k_d^D+k_f^D+k_q} = \frac{k_{ET}}{k_{ET}+{}^1/_{\tau_D}+k_q}, \qquad (4\text{-}4)$$

$$\phi_{qD} = \frac{k_q}{k_{ET}+k_d^D+k_f^D+k_q}, \qquad (4\text{-}5)$$

where $k_d^D$ is the sum of the non-radiative deactivation rate constant and intersystem crossing rate constant of energy donor, $k_f^D$ is the radiative deactivation rate constant of energy donor, $k_q$ is the quenching rate constant from the excited state of donor molecule to ground state of donor or acceptor molecule and $k_{ET}$ is the energy transfer rate constant. In the case of *p*-TMPyP, self-quenching behavior was not observed. Due to observe no quenching with exciting only acceptor in the energy transfer sample at 630 nm (not shown), it was expected that the quenching between the excited acceptor

and the ground state donor did not occur. It is supposed that self-quenching of donor is induced by the quenching reaction in the present system. On the basis of equation (4-3), the fluorescence spectrum $F_{ET}(\nu)$, was simulated with the respective reference fluorescence spectra, $F_D^0(\nu)$ and $F_A^0(\nu)$. Thus, parameters $\eta_{ET}$ and $\phi_{qD}$ can be obtained from the spectral simulation.

Energy transfer experiments were examined under various loading levels. The mol ratio of Fluorone to *p*-TMPyP was 1 to 1 for Fluorone/*p*-TMPyP/clay complex, and the dyes loading were modulated as 0.12, 0.2, 1, 2, 5, 10, 20, 40, 60, 80 and 100 % vs. CEC of the clay. Obtained $\eta_{ET}$ and $\phi_{qD}$ values are plotted vs. the dyes loading level as shown in Figure 4-4. As the loading level increased, the $\eta_{ET}$ increased. These $\eta_{ET}$ were larger than 90% for 20-100% vs. CEC condition and these $\phi_{qD}$ were almost stationary nearly 0% for 0.12-100% vs. CEC. According to Figure 4-4, we can presume the adsorption structure of these dyes on the clay surface. When the adsorption distribution of the adsorbed dyes is uniform and hexagonal, the average intermolecular distance was calculated to be 5.3 nm at 20 % vs. CEC. On the basis of Förster equation (4-1) and 5.3 nm as the intermolecular distance, $k_{ET}$ is calculated to be $4.1\times10^8$ $s^{-1}$ and thus the $\eta_{ET}$ should be 54% ($4.1\times10^8$ $s^{-1}$/($4.1\times10^8$ $s^{-1}$ + $3.5\times10^8$ $s^{-1}$ ($=\tau_D^{-1}$))) without $k_q$, while the actual $\eta_{ET}$ was 93%. Accordingly, dyes are segregated on the clay surface and the actual intermolecular distance between molecules is smaller than that expected by uniform distribution.

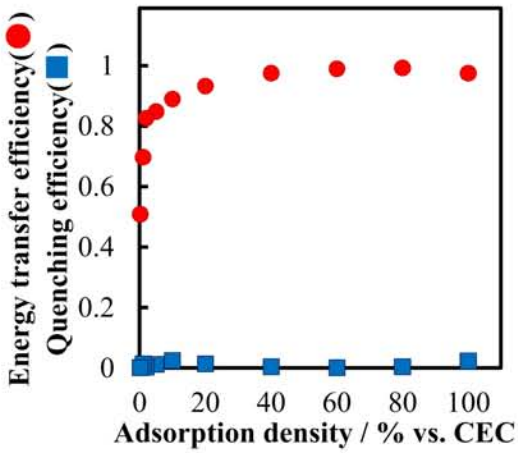


Figure 4-4. Energy transfer efficiency ($\eta_{ET}$) and the quenching efficiency ($\phi_{qD}$) at various loading levels of Fluorone and *p*-TMPyP on the clay surface in water ([Fluorone] = [*p*-TMPyP] = $5.0 \times 10^{-8}$ M). The excitation wavelength was 510 nm.

・***Energy transfer reaction under the various ratio of Fluorone versus p-TMPyP***

The energy transfer efficiency was evaluated under the ratio of [Fluorone] / [*p*-TMPyP] = 1 - 15. From the viewpoint of light harvesting, large [Fluorone] / [*p*-TMPyP] condition is preferable. However, it is expected that, as the ratio of Fluorone increased, the adjacent probability between Fluorone molecules became higher and that between Fluorone and *p*-TMPyP became lower, thus, the self-quenching of Fluorone would occur and energy transfer efficiency became low. The observed energy transfer efficiencies ($\eta_{ET}$) and quenching efficiencies ($\phi_{qD}$) are shown in Figure 4-5. As a result, $\eta_{ET}$ values were larger than 80% at any conditions.

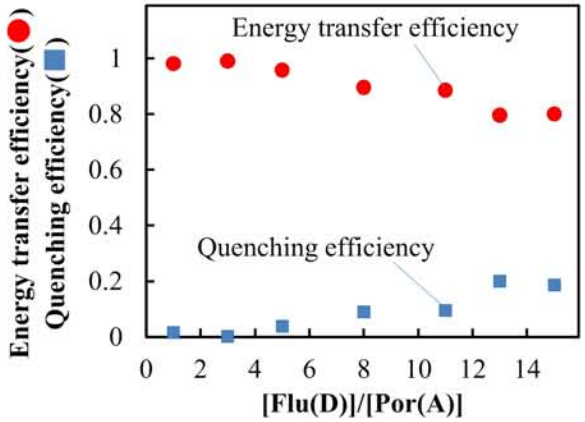


Figure 4-5. The energy transfer efficiency ($\eta_{ET}$) and the quenching efficiency ($\phi_{qD}$) of Fluorone and *p*-TMPyP in water at 100% vs. CEC ([*p*-TMPyP] = 5.0 × $10^{-8}$ M, [Fluorone] = 5.0, 15, 25, 40, 55, 65 and 75×$10^{-8}$ M). The excitation wavelength was 510 nm.

• ***Time-resolved fluorescence measurements for Fluorone/p-TMPyP/clay complex***

To determine the energy transfer rate, the time-resolved fluorescence spectra for Fluorone/*p*-TMPyP/clay complexes were measured. In this experiment, the mol ratio of Fluorone / *p*-TMPyP was set at 1 / 1, and the concentrations of dyes were set at 100% loadings vs. CEC of the clay. The excitation wavelength was set at 510 nm where Fluorone was almost selectively excited.

The normalized time-resolved fluorescence spectra (normalized at 650 nm) for Fluorone/*p*-TMPyP/clay complex are shown in Figure 4-6, and the fluorescence decay profiles of Fluorone/*p*-TMPyP/clay complexes in the region of 550-590 nm and 740-795 nm, corresponding to the fluorescence for Fluorone and *p*-TMPyP, are shown in Figure 4-7. The time-resolved fluorescence spectrum just after excitation (0-50 ps) was same to the Fluorone fluorescence. Fluorescence from

excited *p*-TMPyP appeared and then increased at 650-800 nm region for 50-450 and 450-950 ps. The decay curve at 550-590 nm can be analyzed by three components fitting (Figure 4-7). The lifetimes were calculated to be <30 ps, 0.06 and 0.44 ns with pre-exponential factors of 0.95, 0.04 and 0.01, respectively. The intrinsic excited lifetime of Fluorone without self-quenching and energy transfer reaction was 2.9 ns on the clay surface. The observed lifetimes were apparently shorter than the intrinsic one. The major component (<30 ps) corresponds to that the reaction rate constant is larger than $3.3 \times 10^{10}$ $s^{-1}$. The minor components (0.06 and 0.44 ns) were only 5% of total decay components. These indicate that the adsorption structure of Fluorone/*p*-TMPyP mixture is integrated on the clay surface, and the energy transfer reaction proceeds efficiently. For the decay curve at 740-795 nm (*p*-TMPyP), the rise and decay components were observed. In accordance with the decay of Fluorone fluorescence, the rise of *p*-TMPyP fluorescence was able to be analyzed as very fast component (<30 ps). The decay rate constant for *p*-TMPyP fluorescence was calculated to be 5.1 ns which is similar to that of the *p*-TMPyP/clay complex (5.6 ns). Judging from these results, it is confirmed that the energy transfer proceeds from excited Fluorone to *p*-TMPyP within <30 ps.

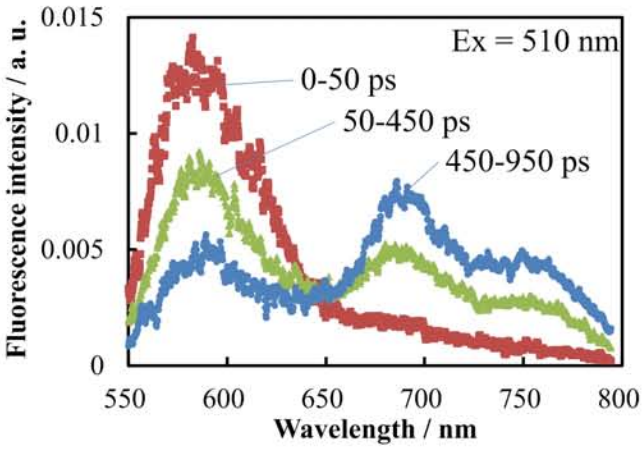


Figure 4-6. Normalized time-resolved fluorescence spectra for Fluorone/*p*-TMPyP/clay complexes at 0~50, 50~450 and 450~950 ps after excitation ([Fluorone] = [*p*-TMPyP] = $5.0 \times 10^{-7}$ M; 100% dyes loadings). The fluorescence intensity was normalized at 650 nm. The excitation wavelength was 510 nm.

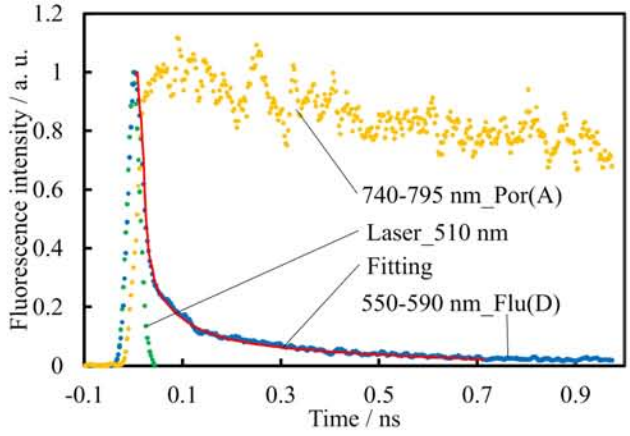


Figure 4-7. Fluorescence decay profiles of Fluorone/*p*-TMPyP/clay complexes in the region of 550~590 nm (blue plot) and 740~795 nm (yellow plot) and fitting curve (red solid line) of it ([Fluorone] = [*p*-TMPyP] = $5.0 \times 10^{-7}$ M; 100% dyes loadings). The excitation wavelength was 510 nm. The laser pulse was indicated by green plot.

・***Energy Transfer Reaction between Fluorone and m-TMPyP***

Fluorescence spectra of dye / clay complexes, where loading level of Fluorone and *m*-TMPyP are 0.05 and 0.05% vs. CEC, respectively, were measured as shown in Figure 4-8. Excitation wavelength was set at 510 nm. Fluorescence spectra of energy transfer sample are shown in Figure 4-9. The dye loading level in this energy transfer sample was 50% vs. CEC. In energy transfer sample, fluorescence from Fluorone (energy donor) decreased and that from *m*-TMPyP (energy acceptor) increased, compared to each reference sample. This indicates that photochemical energy transfer reaction takes place between Fluorone and *m*-TMPyP. By using the fluorescence spectra of Fluorone / clay, *m*-TMPyP / clay and Fluorone and *m*-TMPyP / clay, the energy transfer efficiency ($\eta_{ET}$) and the quenching efficiency of *m*-TMPyP ($\phi_{qA}$) in energy transfer sample can be calculated. The total fluorescence of energy transfer sample can be expressed by equation (4-3).

As a result, $\eta_{ET}$ reached to 82% and $\phi_{qA}$ was 10. Thus, it was turned out that the energy transfer between Fluorone and *m*-TMPyP was efficient.

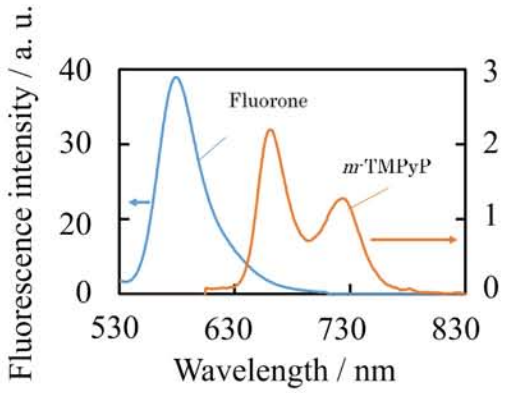

Figure 4-8. Individual fluorescence spectra of Fluorone/clay ([Fluorone] = $5.0 \times 10^{-8}$ M; 0.05% vs. CEC loadings), and *m*-TMPyP/clay ([*m*-TMPyP] = $1.0 \times 10^{-8}$ M; 0.05% vs. CEC loadings) complexes in water. The spectra were measured with excited at 510 nm.

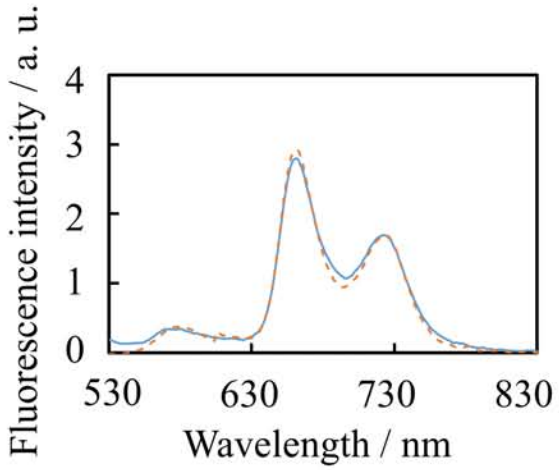


Figure 4-9. The fluorescence spectra of Fluorone/ *m*-TMPyP /clay complex ([Fluorone] = $5.0 \times 10^{-8}$ M, [*m*-TMPyP] = $1.0 \times 10^{-8}$ M; 50% vs. CEC loadings; the solid line) and the sum of fluorescence spectra of Fluorone/clay, *m*-TMPyP/clay and *p*-TMPyP /clay complexes (the dash line). These spectra were measured with excited at 510 nm.

・***Energy transfer reaction under the various ratio of Fluorone versus m-TMPyP***

The energy transfer efficiency was evaluated under the ratio of [Fluorone] / [*m*-TMPyP] = 0.07 - 8. The observed $\eta_{ET}$ and quenching efficiencies $\phi_{qA}$ are shown in Figure 4-10. As a result, $\eta_{ET}$ values were larger than 70% at any conditions. Judging from the decrease of quenching efficiency at large [Fluorone] / [*m*-TMPyP] condition, as the ratio of Fluorone increased, the adjacent probability between *m*-TMPyP molecules became lower and the self-quenching of *m*-TMPyP would be suppressed.

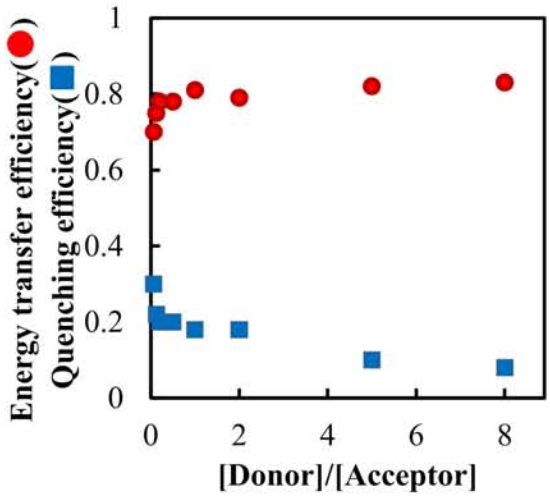


Figure 4-10. The energy transfer efficiency ($\eta_{ET}$) and the quenching efficiency ($\phi_{qA}$) of Fluorone and *m*-TMPyP in water at 50% vs. CEC ([*m*-TMPyP] = $1.0 \times 10^{-8}$ M, [Fluorone] = 0.07, 0.1, 0.2, 0.5, 1.0, 2.0, 5.0 and $8.0 \times 10^{-8}$ M). The excitation wavelength was 510 nm.

### 4-1-4. Conclusion

First, the energy transfer between Fluorone and *p*-TMPyP was measured by using steady state fluorescence spectra. When [Fluorone] / [*p*-TMPyP] = 1, the efficiencies of the energy transfer reaction between Fluorone and *p*-TMPyP at 20-100% vs. CEC were larger than 90%. The maximum energy transfer efficiency was 99%. Judging from the result of time-dependent fluorescence measurement, the energy transfer reaction was very fast ($k_{ET} > 3.3 \times 10^{10}$ $s^{-1}$) at 100% vs. CEC condition. Like these, we achieved efficient energy transfer reaction in clay-dye complexes. Additionally, when [Fluorone] / [*p*-TMPyP] = 15, the energy transfer efficiency ($\eta_{ET}$) was still 80%, despite of a less amount of *p*-TMPyP.

Next, the energy transfer reaction between Fluorone and *m*-TMPyP was evaluated. The energy transfer efficiencies were larger than 70% at [Fluorone] / [*m*-TMPyP] = 0.07 ~ 8. As a result, it was found out that energy transfer reactions from Fluorone to *m*-TMPyP and *p*-TMPyP were efficient.

## 4-2. Energy Transfer Reaction among Three Components

### 4-2-1. Introduction

We have already studied the excited energy transfer reaction between adsorbed two different kinds of dyes on the clay surface. It was reported that the maximum efficiency of the energy transfer from *meso*-tetra (*N*-methyl-3-pyridyl) porphine (*m*-TMPyP) to *meso*-tetra (*N*-methyl-4-pyridyl) porphine (*p*-TMPyP) on the clay surface was ~100%.[31]

We already have evaluated energy transfer reactions between two components. In these case, Fluorone and *m*-TMPyP were energy donor and *p*-TMPyP was energy acceptor. When *m*-TMPyP coexisted with Fluorone, *m*-TMPyP had a behavior as energy acceptor. The energy transfer efficiencies of these systems were summarized in Figure 4-11. This figure indicates that the energy transfer efficiencies depend on the ratio of energy donors to energy acceptors. For example, the efficiency of energy transfer from *m*-TMPyP to *p*-TMPyP tended to decrease with increasing the ratio of *m*-TMPyP to *p*-TMPyP, because the rate of the donor adjacent to acceptor decreased. Judging from these results, the condition in order to achieve the efficient energy transfer reaction among those three components was [Fluorone] > [*p*-TMPyP] > [*m*-TMPyP]. Thus, we supposed that the smallest integer ratio of three components was set to be 3 : 1 : 2 (=[Fluorone] : [*m*-TMPyP] : [*p*-TMPyP]) as the condition in order to fulfill such ratio of three components.

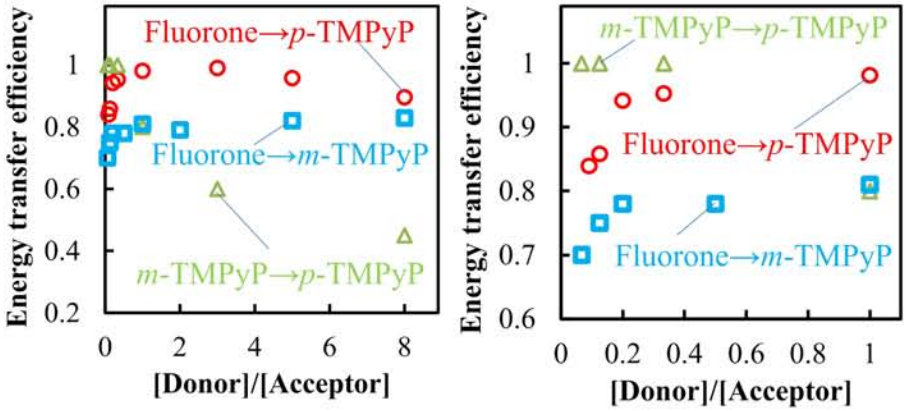


Figure 4-11. Efficiencies of energy transfer between two components. Vertical axis indicates the energy transfer efficiency. Horizontal axis indicates the ratio of energy donor to acceptor. Vertical axis's range of left figure is from 0 to 8, and of right figure is from 0 to 1. The square, circle and triangle indicate the energy transfer efficiencies between Fluorone and *m*-TMPyP, Fluorone and *p*-TMPyP, and m-TMPyP and *p*-TMPyP, respectively.

## 4-2-2. Experimental Section

・***Materials***

*p*-2,4,5,7-tetrakis(*N*-methylpyridinium-4-yl)-6-pottasiumoxy-3-fluorone tetraiodide (Fluorone) was synthesized by the method which was described in the previous section.

・***Preparation methods for the clay/dye complexes***

Typical procedure to prepare energy transfer samples was as follows. In this experiment, Fluorone, *m*-TMPyP, and *p*-TMPyP were used. Aqueous solution of Fluorone, *m*-TMPyP and *p*-TMPyP were mixed. The obtained solutions were mixed with an aqueous clay solution (9.9 mg $L^{-1}$) under vigorous stirring. The total concentrations of Fluorone, *m*-TMPyP and *p*-TMPyP were set at $1.0 \times 10^{-7}$ M, and the clay loadings were changed by changing the concentration of clay. The molar ratio of Fluorone, *p*-TMPyP and *m*-TMPyP was modulated as Fluorone / *m*-TMPyP / *p*-TMPyP = 3/1/2. Under these conditions, the clay sheets exist in a form of individually exfoliated sheets and the obtained solution was substantially transparent.

・***Estimation method of energy transfer efficiency and rate of energy loss***

By using the fluorescence intensities of Fluorone/clay, *m*-TMPyP/clay, *p*-TMPyP/clay and Fluorone/*m*-TMPyP/*p*-TMPyP/clay complexes, the energy transfer efficiency and the loss of the energy transfer was calculated as follows.

The total fluorescence of Fluorone/*m*-TMPyP/*p*-TMPyP/clay complex ($F_{ET}(\nu)$) can be expressed by equation (4-6).

$$F_{ET}(\nu) = \alpha F_f(\nu) + \beta F_m(\nu) + \gamma F_p(\nu) \quad \cdot\cdot\cdot (4\text{-}6)$$

, where $F_f(\nu)$, $F_m(\nu)$ and $F_p(\nu)$ are the fluorescence spectra of Fluorone/clay complex, *m*-TMPyP /clay complex and *p*-TMPyP/clay complex, respectively. $\nu$ is wavelength of fluorescence. $\alpha$, $\beta$ and $\gamma$ indicate ratios of the fluorescence intensity of Fluorone/*m*-TMPyP/*p*-TMPyP/clay complex to the fluorescence intensity of Fluorone/clay complex, *m*-TMPyP/clay complex and *p*-TMPyP/clay complex, respectively. $\alpha$, $\beta$ and $\gamma$ can be shown in equation (4-7), (4-8) and (4-9), respectively.

$$\alpha = 1 - \eta_{fm} - \eta_{fp} - q_f \quad \cdot\cdot\cdot (4\text{-}7)$$

$$\beta = \left(1 + \frac{1-10^{-A_f(\lambda)}}{1-10^{-A_m(\lambda)}}\eta_{fm}\right)\left(1 - \eta_{mp} - q_m\right) \quad \cdot\cdot\cdot (4\text{-}8)$$

$$\gamma = \frac{1-10^{-A_f(\lambda)}}{1-10^{-A_p(\lambda)}}\eta_{fm}\eta_{mp} + \frac{1-10^{-A_f(\lambda)}}{1-10^{-A_p(\lambda)}}\eta_{fp} + \frac{1-10^{-A_m(\lambda)}}{1-10^{-A_p(\lambda)}}\eta_{mp} + 1 \quad \cdot\cdot\cdot (4\text{-}9)$$

, where $\eta_{fm}$, $\eta_{fp}$ and $\eta_{mp}$ are the efficiencies of the energy transfer reaction from Fluorone to *m*-TMPyP and *p*-TMPyP and from *m*-TMPyP to *p*-TMPyP, respectively. $q_f$ and $q_m$ are losses of energy transfer at Fluorone and *m*-TMPyP, respectively.$A_f(\lambda)$, $A_m(\lambda)$ and $A_p(\lambda)$ are absorbance of Fluorone/clay complex, *m*-TMPyP /clay complex and *p*-TMPyP/clay complex at excitation wavelength ($\lambda$), respectively. $F_{ET}(\nu)$,

$F_f(\nu)$, $F_m(\nu)$ and $F_p(\nu)$ were measured at different two excitation wavelength (520 and 540 nm). On the basis of equation (4-6), the fluorescence spectrum $F_{ET}(\nu)$, was simulated with the use of the respective reference fluorescence spectra $F_f(\nu)$, $F_m(\nu)$ and $F_p(\nu)$. Using obtained two kinds of coefficients by measuring fluorescence spectra, simultaneous equations are solved and parameters which the energy transfer efficiencies and the loss of the energy transfer can be obtained from the spectral simulation.

The energy harvesting functionality was evaluated by observed $\gamma$ ($\gamma_{obs}$). $\gamma_{obs}$ was calculated by using observed energy transfer efficiencies such as $\eta_{fm}$, $\eta_{fp}$ and $\eta_{mp}$. When $\gamma_{obs}$ is larger than 1, the excitation frequency of *p*-TMPyP in this energy transfer system increase as compared with it of only *p*-TMPyP.

### 4-2-3. Results and Discussion

・ ***Energy transfer reaction in Fluorone/m-TMPyP/p-TMPyP/clay complex***

At first, the absorption spectrum of Fluorone/*m*-TMPyP/*p*-TMPyP/clay complex was measured, and it was found out that the spectrum was completely identical with a sum of individual absorption spectra of Fluorone/clay, *m*-TMPyP/clay and *p*-TMPyP/clay complexes as shown in Figure 4-12. Thus, it was found out that an aggregation is completely suppressed and the dye molecules exist as a single molecule even when three types of dye co-exist on the clay surface.

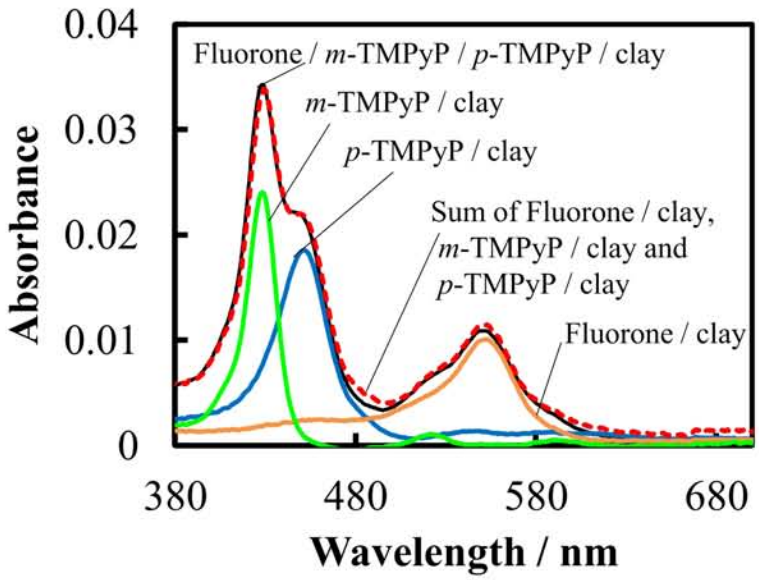


Figure 4-12. The absorption spectra of Fluorone/clay ([Fluorone] = $1.0 \times 10^{-7}$ M, 20% vs. CEC; orange line), *m*-TMPyP /clay ([*m*-TMPyP] = $1.0 \times 10^{-7}$ M, 20% vs. CEC; green line), *p*-TMPyP. /clay ([*p*-TMPyP] = $1.0 \times 10^{-7}$ M, 20% vs. CEC; blue line), a sum of individual absorption spectra of them (red broken line) and co-adsorption sample ([Fluorone] = [*m*-TMPyP] = [*p*-TMPyP] = $1.0 \times 10^{-7}$ M, 20% vs. CEC; black line).

The energy transfer between Fluorone, *m*-TMPyP and *p*-TMPyP on the clay surface was examined by measuring steady-state fluorescence spectra. Individual fluorescence spectra of Fluorone/clay, *m*-TMPyP/clay and *p*-TMPyP/clay complexes are shown in Figure 4-13. The dye loadings were 0.05% vs. CEC for individuals. By using individual fluorescence spectra, the energy transfer efficiency and loss of energy transfer were given with using equation (4-6) ~ (4-9). For example, the fluorescence spectrum of Fluorone/*m*-TMPyP/*p*-TMPyP/clay complex, where its total dye loading was set at 40% vs. CEC for Fluorone/*m*-TMPyP/*p*-TMPyP/clay complex, was shown in Figure 4-14. The mol ratio of Fluorone : *m*-TMPyP : *p*-TMPyP was set at 3 : 1 : 2 in Fluorone/*m*-TMPyP/*p*-TMPyP/clay complex. The fluorescence spectral shape of energy transfer sample can be fit by the linear combination of individual fluorescence spectra as shown in Figure 4-14. In order to evaluate the energy transfer efficiency and loss of energy transfer in three components, the fluorescence spectra of energy transfer samples were measured at deferent two excitation wavelengths. The excitation wavelengths were set at 520 and 540 nm.

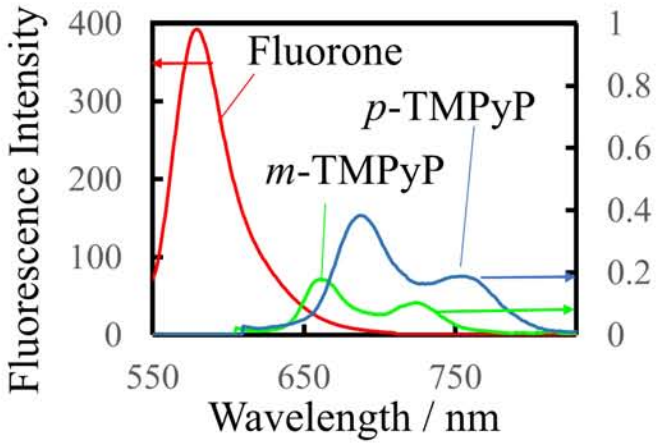


Figure 4-13. Individual fluorescence spectra of Fluorone/clay ([Fluorone] = $5.0 \times 10^{-8}$ M; 0.05% vs. CEC), *m*-TMPyP/clay ([*m*-TMPyP] = $1.7 \times 10^{-8}$ M; 0.05% vs. CEC) and *p*-TMPyP/clay ([*p*-TMPyP] = $3.3 \times 10^{-8}$ M; 0.05% vs. CEC) complexes in water. The spectra were measured with excited at 540 nm.

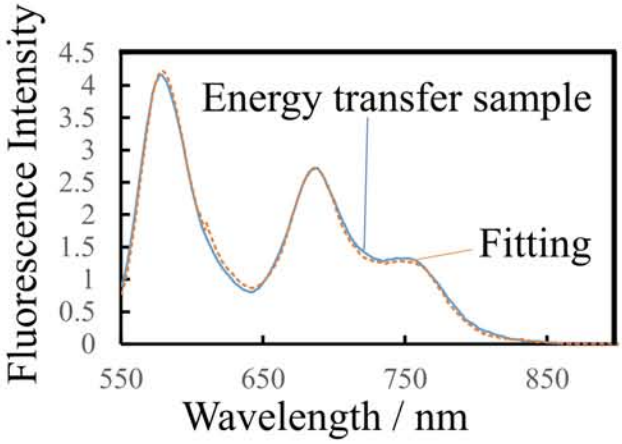


Figure 4-14. Fluorescence spectra of Fluorone / *m*-TMPyP / *p*-TMPyP / clay complex ([Fluorone] = $5.0 \times 10^{-8}$ M, [*m*-TMPyP] = $1.7 \times 10^{-8}$ M, [*p*-TMPyP] = $3.3\times 10^{-8}$ M; The total dye loading was 40% vs. CEC; the solid line) and the sum of fluorescence spectra of Fluorone/clay, *m*-TMPyP/clay and *p*-TMPyP /clay complexes (the dash line). The spectra was measured with excited at 540 nm.

Energy transfer efficiencies were evaluated by changing the loading level. The mol ratio of Fluorone : *m*-TMPyP : *p*-TMPyP was set at 3 : 1 : 2 in Fluorone/*m*-TMPyP/*p*-TMPyP/clay complex and the dye loadings were modulated as 1, 5, 10, 20, 30, 40, 50 and 70% vs. CEC of the clay. Obtained energy loss are plotted in Figure 4-15. Obtained energy transfer efficiencies are plotted vs. the dyes loading level as shown in Figure 4-16.

The losses of energy transfer among Fluorone, m-TMPyP and p-TMPyP were shown in Figure 4-15. The loss of energy transfer from *m*-TMPyP was almost 0% and the loss of energy transfer from Fluorone was increased, when the loading level increased. It was supposed that this energy loss was caused by the collision between an excited Fluorone and a ground state Fluorone on the clay surface. In this system, the number of Fluorone molecules was larger than the number of Porphyrins. Then, when the dye molecules adsorbed on the clay surface, the numbers of the adjacent Fluorone to Fluorone on the clay surface tended to be large and the energy loss became large.

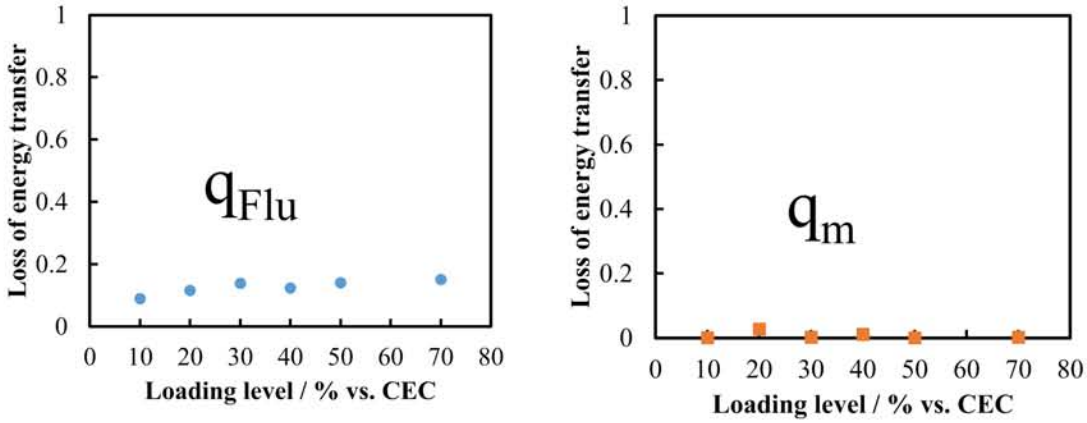


Figure 4-15. Obtained values of the energy loss at various loading levels of Fluorone, *m*-TMPyP and *p*-TMPyP ([Fluorone] = $5.0 \times 10^{-8}$ M, [*m*-TMPyP] = $1.7 \times 10^{-8}$ M, [*p*-TMPyP] = $3.3 \times 10^{-8}$ M; 10~70% loadings vs. CEC). Left figure shows the energy loss of Fluorone and right figure shows it of *m*-TMPyP.

The efficiencies of the energy transfer from Fluorone ($\eta_{fm} + \eta_{fp}$) were 80~90% for 10~70% loadings vs. CEC. The maximum value of $\eta_{fm} + \eta_{fp}$ is 1. The efficiency of the energy transfer from *m*-TMPyP to *p*-TMPyP ($\eta_{mp}$) was also larger than 70% for 10~70% loadings vs. CEC. These results were similar to the energy transfer between only two components. They indicate that dye molecules adsorb on the clay surface without separation of dyes in the energy transfer sample. In this system, the number of Fluorone molecules was larger than the number of Porphyrins. Then, when the dye molecules adsorbed on the clay surface, the numbers of the adjacent Fluorone to Fluorone on the clay surface tended to be large and the energy loss became large. The rate constant of Förster type energy transfer reaction is proportional to the sixth power of the distance from the center of energy donor molecule to that of energy acceptor molecule. Because the average distance between donor and the adjacent

acceptor molecule on the clay surface became small by increasing the adsorption density of porphyrins on the clay surface, the frequency of the energy transfer increased with increasing the adsorption density. As shown in Figure 4-16, the energy transfer efficiencies were not almost changed at high dye loadings. It indicates that adsorbed dye molecules assembled and segregated on the clay surface.

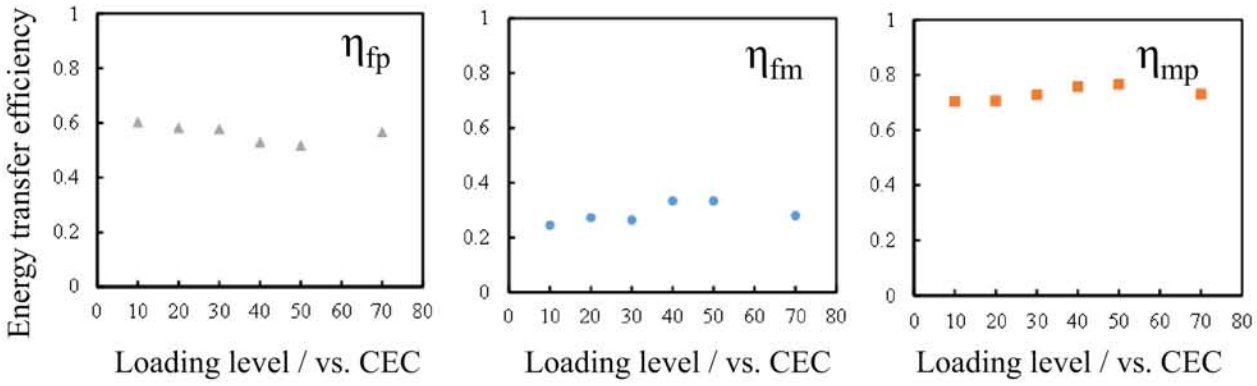


Figure 4-16. Obtained values of the energy transfer efficiency at various loading levels of Fluorone, *m*-TMPyP and *p*-TMPyP ([Fluorone] = $5.0 \times 10^{-8}$ M, [*m*-TMPyP] = $1.7 \times 10^{-8}$ M, [*p*-TMPyP] = $3.3 \times 10^{-8}$ M; 10~70% loadings vs. CEC). Left figure shows the efficiency of the energy transfer from Fluorone to *p*-TMPyP, center figure shows it from Fluorone to *m*-TMPyP and right figure shows it from *m*-TMPyP to *p*-TMPyP.

・***Evaluation of the enhancement ratio of excitation frequency $\Gamma_{380\text{-}780\ nm}$***

$\gamma_{obs}(\lambda)$ was evaluated by using equation (4-9) and observed energy transfer efficiencies. $\gamma_{obs}(\lambda)$ values indicate how much excitation frequency of *p*-TMPyP in energy transfer system is larger than it in only *p*-TMPyP/clay complex at $\lambda$. $\lambda$ indicates excitation wavelength (nm). $\gamma_{obs}(\lambda)$ is shown in Figure 4-17. The maximum $\gamma_{obs}(\lambda)$ was 38 at 513 nm excitation. It indicates that Fluorone absorbs incident light, where porphyrin cannot efficiently absorb, and transfers excitation energy to *p*-TMPyP. If this system is used for a photochemical reaction, the reaction frequency will be larger than it without this energy transfer system. However, the result with a specific wavelength excitation was not enough to evaluate the light harvesting performance. Therefore, we newly suppose the novel evaluation method for the light harvesting performance. An important role of light harvesting system is the concentration of sunlight energy into the photoreaction center. Thus, the light harvesting functionality should be evaluated by $\Gamma_{380\text{-}780\ nm}$. $\Gamma_{380\text{-}780\ nm}$ was the ratio of excitation frequency and was defined in terms of the equation 4-10.

$$\Gamma_{380-780\ nm} = \frac{\int_{780}^{380} \gamma_{obs}(\lambda)\left(1-10^{-A_p(\lambda)}\right)N_{sunlight}(\lambda)d\lambda}{\int_{780}^{380}\left(1-10^{-A_p(\lambda)}\right)N_{sunlight}(\lambda)d\lambda} \qquad (4\text{-}10)$$

, where $N_{sunlight}(\lambda)$ ($m^{-2}$ $s^{-1}$ $nm^{-1}$) indicates the photon number of sunlight spectrum[49] in AM1.5 at $\lambda$ and $A_p(\lambda)$ indicates the absorbance of *p*-TMPyP at $\lambda$ in this system. $\Gamma_{380\text{-}780\ nm}$ indicates the ratio of the excitation frequency of *p*-TMPyP in this light harvesting system (Fluorone, *m*-TMPyP and *p*-TMPyP/clay system) divided by that in only *p*-TMPyP/clay system. When [*p*-TMPyP] = $3.3 \times 10^{-8}$ M, $\int_{780}^{380}\left(1-10^{-A_p(\lambda)}\right)N_{sunlight}(\lambda)d\lambda$ was calculated to be $1.9 \times 10^{18}$ $m^{-2}$ $s^{-1}$. Calculated results of

this integral and $\Gamma_{380\text{-}780\ nm}$ should depend on the concentration of samples. When the concentration of dyes in energy transfer samples increased, $\Gamma_{380\text{-}780\ nm}$ should become smaller than that in the dilute condition due to the saturation of light absorption rate. In this system, energy transfer reaction was evaluated at the dilute concentration in order to neglect the energy transfer by the trivial mechanism and the internal filter effect. In the present light harvesting system, $\Gamma_{380\text{-}780\ nm}$ was calculated to be 2.4. In other words, the excitation frequency of *p*-TMPyP became 2.4 times higher by the effect of this artificial LHS. Judging from Figure 4-17, $\Gamma_{380\text{-}780\ nm}$ will be larger than 2.4 with adding the dye, which absorbs the light region of 380-480, and 580-780 nm to this system.

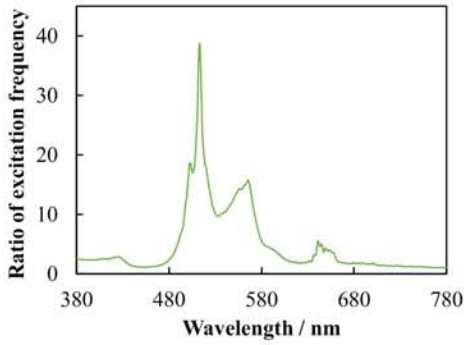


Figure 4-17. Ratio of excitation frequency $\gamma_{obs}(\lambda)$ of Fluorone/ *m*-TMPyP / *p*-TMPyP /clay complex ([Fluorone] = $5.0 \times 10^{-8}$ M, [*m*-TMPyP] = $1.7 \times 10^{-8}$ M, [*p*-TMPyP] = $3.3 \times 10^{-8}$ M; 40% loadings vs. CEC).

### 4-2-4. Conclusion

In the present chapter, the quantitative excited singlet multiple-step energy transfer reaction among adsorbed three kinds of dyes on the clay surface was successfully achieved. Additionally, the energy transfer efficiencies of these multiple-step processes were analyzed using novel analysis formulae. The efficiency of energy transfer from Fluorone to *m*-TMPyP and *p*-TMPyP was 90% and from *m*-TMPyP to *p*-TMPyP was 75% when the total dye loading is 40% vs. CEC of the clay. Judging from these results, clay/porphyrin complexes are promising candidates as an efficient artificial LHS.

Additionally, we newly propose the parameter $\Gamma_{380\text{-}780\ nm}$ in order to evaluate the performance of the artificial LHS. $\Gamma_{380\text{-}780\ nm}$ indicates the ratio of the excitation frequency of energy acceptor in LHS to it without energy donor by sunlight irradiation. In the present system, $\Gamma_{380\text{-}780\ nm}$ was calculated to be 2.4 and we achieved to increase the excitation frequency of energy acceptor with using this artificial LHS.

# 5. Light-Harvesting Reaction

One of LHS functionalities is concentration of sunlight energy for the phototochemical reaction center. Therefore I will be construct the energy transfer system which collects the sunlight energy by using long range and anisotropic energy transfer.

## 5-1. Energy Migration Reaction

### 5-1-1. Introduction

In this section, I aim to develop the energy transfer system by the use of dye where an energy migration reaction is possible in the dye-clay system. I investigated the energy transfer reaction from Fluorone to *p*-TMPyP as shown in chapter 4. When the energy transfer efficiency ($\eta_{ET}$) was evaluated under the ratio of [Fluorone] / [*p*-TMPyP] = 1 – 15, $\eta_{ET}$ values were larger than 80% at any conditions. If the theoretical adsorption structure of Fluorone and *p*-TMPyP on the clay surface is supposed, there are non-adjacent donors to an acceptor at [Fluorone] / [*p*-TMPyP] = 15 condition. And then, the energy transfer efficiency from the non-adjacent donor to acceptor should be low. Because the rate constant of the energy transfer became small due to the long distance between donor and acceptor.

However, in this system, the long range energy transfer reaction took place efficiently with energy migration between the donor molecules. The conditions for efficient energy migration reaction are 1) the large spectral overlap (*J*) between the fluorescence and absorption spectrum of energy donor and 2) the distance between energy donor molecules is enough smaller than $R_0$. $R_0$ is called the Förster radius and is the distance where energy transfer rate and deactivation rate is equal. Fluorone has the

large spectral overlap ($J = 2.9 \times 10^{-13}$ $M^{-1}$ $cm^3$ and $R_0$ is 6.1 nm) and the typical distance between Fluorone is 2.4 nm, thus, the efficient energy migration between Fluorone molecules is expected.

## 5-1-2. Experimental section

・***Materials***

Fluorone was synthesized according to the before chapter.

・***Preparation for Fluorone/p-TMPyP/clay complexes for energy transfer reaction measurements***

Typical procedure to prepare energy transfer samples was as follows. In this experiment, Fluorone and *p*-TMPyP were used as an energy donor and an energy acceptor, respectively. Aqueous solution of Fluorone and *p*-TMPyP were mixed. The obtained solutions were mixed with an aqueous clay solution (9.9 mg $L^{-1}$) under vigorous stirring. When the molar ratio of Fluorone to *p*-TMPyP was 1.0, the total concentrations of Fluorone and *p*-TMPyP were set at $1.0 \times 10^{-7}$ M and the clay loadings were changed by changing the concentration of clay. For Donor/Acceptor ratio (D/A) changing experiments, the concentrations of *p*-TMPyP was set at $5.0 \times 10^{-8}$ M and those of Fluorone were 5.0, 15, 25, 40, 55, 65 and $75 \times 10^{-8}$ M. The total dye loadings were set at 100% vs. CEC by the changing the concentration of clay.

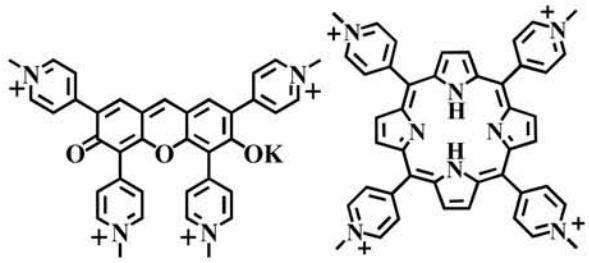

Figure 5-1. The structures of *p*-2,4,5,7-tetrakis(*N*-methylpyridinium-4-yl)-6-pottasiumoxy-3-fluorone tetraiodide (Fluorone; left) and *p*-tetrakis(*N*-methylpyridinium-4-yl) porphyrin tetrachloride (*p*-TMPyP; right).

## 5-1-3. Results and discussion

• ***Fluorescence self-quenching behavior of Fluorone in Fluorone/clay complexes***

The fluorescence self-quenching behavior of Fluorone on the clay surface was examined by measuring the fluorescence quantum yields ($\phi_f$) at various loading level of Fluorone, prior to the energy transfer experiment. The self-quenching decreases the excited singlet lifetime of the dye, and thus, decreases the energy transfer efficiency. To construct the efficient energy transfer systems, understanding the self-quenching behavior is essential. As reported before, the self-quenching of *p*-TMPyP was not observed on the clay surface even at a high density adsorption condition (not shown). On the other hand, a significant self-quenching was observed for typical dyes on the clay surface. Such self-quenching was induced by a collisional reaction such as an electron transfer from an excited molecule to the adjacent ground state molecule.

Under the present experimental condition, the concentration of Fluorone is always kept constant to be $1.0 \times 10^{-7}$ M and the loading level of adsorption was varied by controlling the concentration of

clay. The observed $\phi_f$ for Fluorone/clay complexes, when their loading level were changed from 0.025% to 100% vs. CEC, are shown in Figure 3-11. The fluorescence below 0.06% adsorption can be used as the intrinsic fluorescence intensity because almost same $\phi_f$ at 0.025 and 0.6% loadings indicates that the self-quenching is negligible under these conditions (Figure 3-11 inset). As the Fluorone loading level increased, the $\phi_f$ decreased significantly as can be seen in Figure 3-11.

The $\phi_f$ of Fluorone/clay complex ($\phi_D$) was 0.49 at 0.06% vs. CEC. At 100% loadings, the $\phi_f$ of Fluorone/clay complex ($\phi'_D = 0.013$) was 0.027 times as large as $\phi_D(0.49)$. The excited lifetime for Fluorone/clay complex is 2.9 ns ($\tau_D$) as reported in previous chapter. Then, the rate constant of self-quenching between Fluorone molecules ($k_q$) at 100% loadings was calculated to be $1.2 \times 10^{10}$ $s^{-1}$ according to equation (5-1) and (5-2). For an efficient energy transfer reaction, the energy transfer rate ($k_{ET}$) should be enough larger than $k_q$. It should be noted that this $k_q$ value is assumed maximum value as the absence of acceptor.

$$\phi_D = \frac{k_f}{1/\tau_D} \quad (5\text{-}1),$$

$$\phi'_D = \frac{k_f}{k_q + 1/\tau_D} \quad (5\text{-}2),$$

The energy transfer rate constant $k_{ET}$ can be theoretically calculated by using Förster equation (4-1).

According to the analysis of the overlap between the fluorescence of Fluorone and the absorption of *p*-TMPyP, based on equation (4-2), the spectral overlap integral $J$ is calculated to be $1.6 \times 10^{-13}$ $M^{-1}cm^{-1}cm^4$. $k_{ET}$ was calculated to be $5.0 \times 10^{10}$ $s^{-1}$ by using equation (4-2). This $k_{ET}$ value is sufficiently larger than $k_q$ for efficient energy transfer reaction.

・***Efficient Energy Transfer in the Excessive Donor Condition***

The obtained $\eta_{ET}$ at chapter 4-1 was compared with the theoretical $\eta_{ET}$ to discuss the detail of energy transfer pathway. This theoretical value was calculated based on the hexagonal array of molecules as described below. The schematic representation for possible ideal adsorption structure under [Fluorone] / [*p*-TMPyP] = 15 is shown at the left of Figure 5-2. In the figure, the open square (□), the black closed circle (●), the gray closed circle (●), and the open circle (○) indicate the acceptor (*p*-TMPyP), the primary neighboring donor, the secondary neighboring donor, and the thirdly neighboring donor (Fluorone) to the acceptor, respectively.

Based on the intermolecular distance and the number of neighboring molecules (N), the theoretical $\eta_{ET}$ between each donor-acceptor pairs can be calculated. The center-to-center distance between primary adjacent Fluorone(●) and *p*-TMPyP(□) at 100% vs CEC condition is calculated to be 2.4 nm, and $k_{ET}$ for adjacent Fluorone and *p*-TMPyP pair is calculated to be $5.0 \times 10^{10}$ $s^{-1}$ according to eq (3). On the other hand, the self-quenching rate constant ($k_q$) is $1.2 \times 10^{10}$ $s^{-1}$ at 100% vs. CEC as described in previous chapter. By using this $k_{ET}$ and $k_q$ value, and $\tau_D$ (2.9 ns), the theoretical $\eta_{ET}$ is calculated to be 80% under [Fluorone] / [*p*-TMPyP] = 15 and 100% vs CEC condition, according to equation (4-4). The distance between secondary adjacent Fluorone(●)− *p*-TMPyP(□) pair is calculated to be 4.2 nm under 100% CEC condition. $k_{ET}$ for the secondary adjacent Fluorone− *p*-TMPyP pair is calculated to be $1.7 \times 10^9$ $s^{-1}$. The theoretical $\eta_{ET}$ is calculated to be 12%. In addition, the distance between thirdly adjacent Fluorone(○)−*p*-TMPyP(□) pair is calculated to be 4.8 nm under

100% vs. CEC condition. At this intermolecular distance, the theoretical $k_{ET}$ and $\eta_{ET}$ for the thirdly adjacent Fluorone−*p*-TMPyP pair are calculated to be $1.6 \times 10^9$ $s^{-1}$ ( = $k_{ET}^0$ × N, where $k_{ET}^0$ is energy transfer rate constant considering one energy acceptor ($7.8 \times 10^8$ $s^{-1}$) and N is a number of acceptor molecules that are at the distance of 4.8 nm from a donor molecule (N=2 in this case)) and 11%, respectively. When the distance between Fluorone and *p*-TMPyP is longer than 4.8 nm, the theoretical $\eta_{ET}$ will be lower than 10%. Thus, the condition that the energy transfer reaction at longer intermolecular distance than 4.8 nm was neglected.

Based on the ideal adsorption structure shown in the left of Figure 5-2, the ratio of primary, secondary and thirdly neighboring Fluorone is 40%(●: intermolecular distance is 2.4 nm), 40%(●: intermolecular distance is 4.2 nm) and 20%(○: intermolecular distance is 4.8 nm) in the unit lattice, respectively. Thus, the theoretical $\eta_{ET}$ under [Fluorone] / [*p*-TMPyP] = 15 condition is calculated to be 39% (=0.4 × 80% + 0.4 × 12% + 0.2 × 11%). The observed $\eta_{ET}$ (80%) under Fluorone / *p*-TMPyP = 15 condition is apparently higher than the theoretical $\eta_{ET}$ (39%). The experimentally obtained $\eta_{ET}$ of this system (80%) was nearly equal to the theoretical efficiency of the energy transfer from primary neighboring Fluorone to the adjacent *p*-TMPyP (80%).

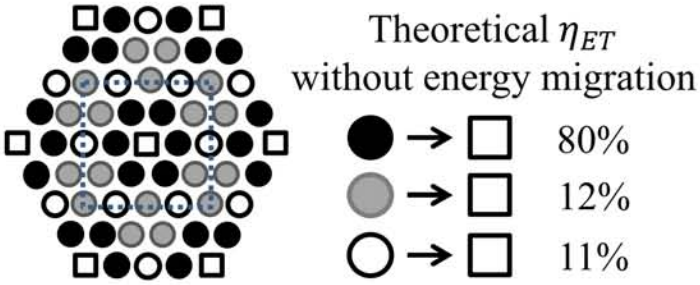


Figure 5-2. (Left) Possible idealized adsorption structure model under [Fluorone]/[*p*-TMPyP] = 15/1 condition on the basis of a hexagonal array. □ indicates the *p*-TMPyP molecule, ● indicates the Fluorone molecule which neighbors the *p*-TMPyP molecule, and ● and ○ indicate the Fluorone molecules which do not neighbor the *p*-TMPyP molecule. Rectangle shown by dotted line indicates the unit lattice. (Right) Theoretical $\eta_{ET}$ between each donor-acceptor pairs.

To explain why the observed $\eta_{ET}$ was higher than the theoretical one, the possibility of energy migration between donor molecules is discussed below. According to the Förster equation (eq (4-1)), the rate constant for energy migration between Fluorone molecules was calculated to be $9.2 \times 10^{10}$ $s^{-1}$ by using $J$ value as $2.9 \times 10^{-13}$ $M^{-1}$ $cm^3$. This theoretical energy migration rate constant is much faster than the deactivation ($\tau_D^{-1}$ = $3.5 \times 10^8$ $s^{-1}$), energy transfer ($k_{ET}$ = $1.7 \times 10^9$ and $1.6 \times 10^9$ $s^{-1}$), and the self-quenching reaction ($k_q$ = $1.2 \times 10^{10}$ $s^{-1}$).

If the energy migration occurs between Fluorone molecules, the anisotropy of Fluorone's fluorescence should decrease as frequency of energy migration increases. The fluorescence spectra of Fluorone adsorbed on the clay surface and its anisotropy were measured at 0.1, 2.5, and 40% vs CEC adsorption conditions. As a result, the anisotropy decreased as the adsorption density of Fluorone

increased on the clay surface as shown in Figure 5-3 and Table 5-1. This result indicates that there is energy migration between Fluorone molecules on the clay surface. It is turned out that the energy migration due to the large *J* between donor molecules enhances the energy transfer efficiency in the present system.

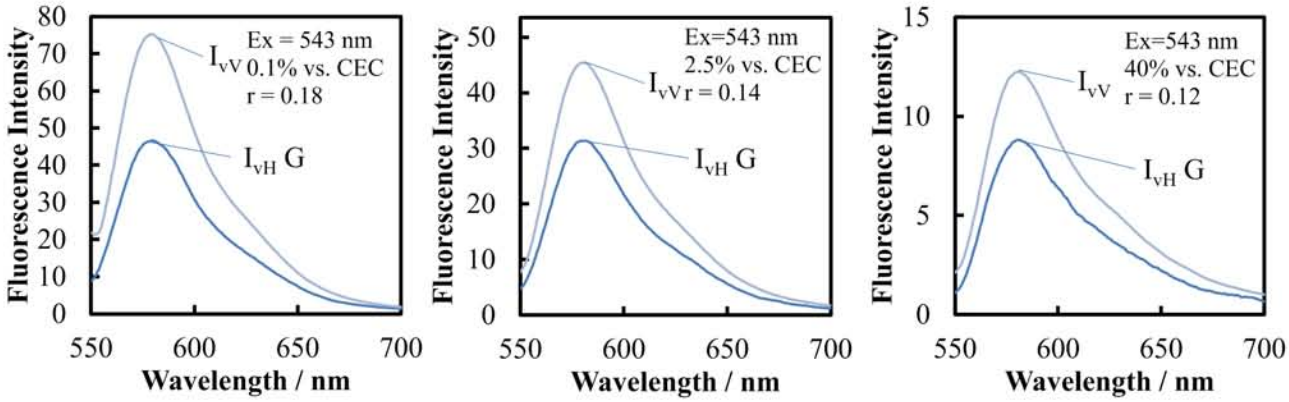


Figure 5-3. The polarized fluorescence spectra of Fluorone with clay in water. [Fluorone] = $1.0 \times 10^{-7}$ M, The adsorption densities of Fluorone are 0.1, 2.5 and 40% vs. CEC of clay.

Table 5-1. The fluorescence anisotropy and lifetime of Fluorone with clay in water. [Fluorone] = $1.0 \times 10^{-7}$ M, The adsorption densities of Fluorone are 0.1, 2.5 and 40% vs. CEC of clay.

| Loading level / % vs. CEC | 0.1 | 2.5 | | 40 | | |
|---|---|---|---|---|---|---|
| *r* | **0.18** | **0.14** | | **0.12** | | |
| components | 1 | 1 | 2 | 1 | 2 | 3 |
| Lifetime | 2.7 ns | 0.4 ns | 2.4 ns | 0.2 ns | 0.7 ns | 2.1 ns |
| Ratio of components | 1 | 0.36 | 0.64 | 0.51 | 0.24 | 0.25 |

### 5-1-4. Conclusion

The photochemical energy transfer reaction on the clay surface between Fluorone and *p*-TMPyP was investigated. When [Fluorone]/[*p*-TMPyP] = 15, the energy transfer efficiency ($\eta_{ET}$) was still 80%, despite of a less amount of *p*-TMPyP. Judging from this observed $\eta_{ET}$ and theoretically calculated one, the occurrence of long range energy transfer reactions due to the energy migration between Fluorone molecules is expected. Fluorescence anisotropy observation of Fluorone supported this speculation. In this study, we found out that the efficient light harvesting type energy transfer system that equips the energy migration functionality can be constructed by using the system where J values between donor-donor and donor-acceptor are large. The concept obtained in this study can unfold options of strategies to construct the artificial light harvesting system that collects and concentrates the sunlight energy efficiently.

## 5-2. Anisotropic Energy Transfer Reaction

### 5-2-1. Introduction

I have been studying the photo-functionality of the complex composed of dyes and nano-sheets such as clay minerals. So far, these researches have been limited for the application in solution system where clay nano-sheets exfoliate and exist as a single sheet in aqueous condition. For the use as functional materials, three-dimensional solid system such as membrane is preferred. In the membrane system, inter-sheet energy transfer in addition to intra-sheet energy transfer should be possible, which enables anisotropic energy transfer. Such inter-sheet energy transfer system has been reported by using the membrane prepared by Layer by Layer (LbL) and Langmuir-Blodgett (LB) technique[50, 51]. However, the assembly structure of dyes in the membrane has been not clear and been difficult to control in those researches. In this study, we combined the assembly structure control technique (Size-matching effect) and LB technique for the preparation of ideal three-dimensional system and examined the anisotropic inter-sheet energy transfer reaction. The preparation and characterization of LB membrane containing porphyrin dyes and the detail of energy transfer reaction in the LB membrane were described.

## 5-2-2. Experimental Section

・***Materials***

Chloroform, methyl alcohol, concentrated sulphuric acid, hydrogen peroxide and sodium chloride was purchased from Kanto Chemical Co., Inc. Dimethyldistearylammonium chloride（DSA）was purchased from Tokyo Chemical Industry Co., Ltd. The glass substrate (slide glass (S011110), thickness is 0.8～1.0 mm) was purchased from Matsunami Glass Ind., Ltd. The Glass plate (3 cm×1.4 cm) was washed by piranha solution ($H_2O_2/H_2SO_4$ = 3/7 (v/v)) just before use.

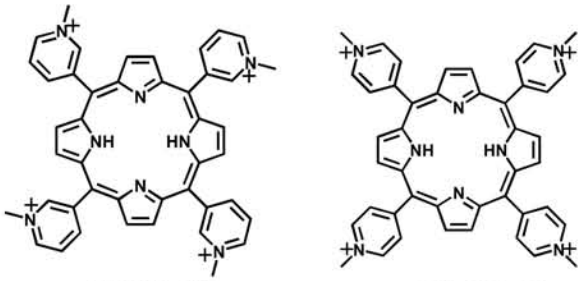


*m*-TMPyP　　*p*-TMPyP

Figure 5-4. Structure of tetrakis(1-methylpyridinium-3-yl) porphyrin (*m*-TMPyP) and tetrakis(1-methylpyridinium-4-yl) porphyrin (*p*-TMPyP).

・***Analysis***

A quartz cell was used in absorption measurements. When fluorescence spectra were measured, a plastic cell (PMMA) was used and a 550 nm long pass filter was set in front of detector. In atomic force microscopy measurement (AFM mode), SPI4000 and SPA300HV systems (SII Nano-Technology Inc.) were used, and AF-40 (SII Nano-Technology Inc.) was used as a cantilever.

## 5-2-3. Results and discussion

・***Preparation of porphyrin-SSA LB film***

Clay LB membrane on the glass plate was prepared according to the literature[52, 53]. The stock solution of DSA (0.2 mM) was prepared in methanol-chloroform (1/9 (v/v)). The DSA solution 100 μL was spread onto the SSA aqueous solution ($1.0\times10^{-5}$ equiv. $L^{-1}$) in LB trough (KSV NIMA). After standing it for 15 min to evaporate the organic solvents and to form a clay-DSA hybrid layer film at room temperature, the floating monolayer was transferred onto the hydrophilic glass plate at 15 mN $m^{-1}$ surface pressure by vertical lifting method (lifting speed 1 mm $min^{-1}$). The obtained membrane on the glass plate was dried at 300℃ for 8 hours. The membrane was washed with saturated NaCl solution in $CHCl_3$/MeOH (4/5 (v/v)) to remove surfactant on the LB clay surface. Then, the membrane was washed with water and dried under vacuum. The AFM image of obtained LB membrane is shown in Figure 5-5. Judging from the image, the surface is quite flat and clay sheets are densely packed as monolayer. The coverage was calculated to be c.a. 95%.

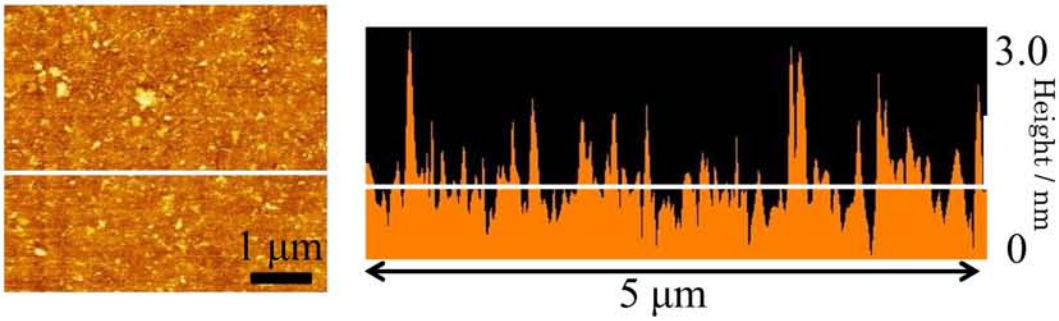


Figure 5-5. AFM image of LB membrane composed of SSA on a glass plate.

The obtained LB membrane on a glass plate was immersed in aqueous porphyrin solution for 24 hours to obtain LB membrane-porphyrin complex. The concentration of the porphyrin was $7.8\times10^{-8}$ M corresponds to 40% vs. CEC of the clay. Considering the usage of half surface for the adsorption, this coverage corresponds to 80% vs. CEC (0.16 molecules $nm^{-2}$). The obtained porphyrin/SSA membrane is named as LB (1) where the number in parenthesis is a number of layer. By repeating this procedure, LB (1-4) were prepared.

Absorption spectra of LB (1-4) of *m*-TMPyP are shown in Fig. 5-6 (a). The spectral shape is identical for all samples and Lambert-Beer type plot at 428 nm showed linear relationship (Fig. 5-6 (b)). These observations indicate that porphyrin-SSA layer was successfully stacked by this technique. The image of LB (4) is shown in Fig. 5-6 (c).

(a) (b) (c)

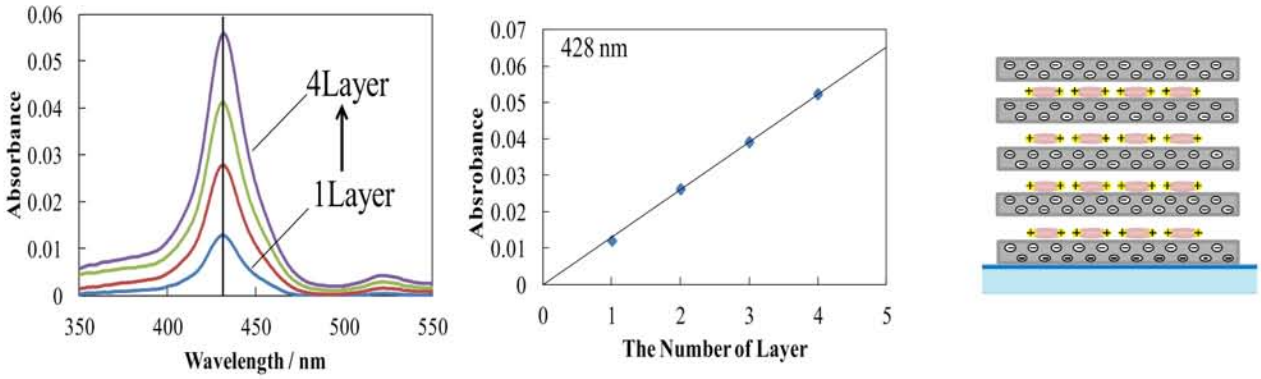


Figure 5-6. (a) Absorption spectra of LB (1-4). (b) Absorbance at 428 nm for LB (1-4). (c) Image for the structure of LB (4).

・***Energy transfer reaction in the p-TMPyP / m-TMPyP LB membranes***

In this study, *m*-TMPyP and *p*-TMPyP were used as energy donor and acceptor, respectively. By using LB technique, clay / *m*-TMPyP / clay / glass and *p*-TMPyP / clay / glass structure were prepared as reference sample. Those are named as LB (*m*) and LB (*p*), respectively. For the preparation of energy transfer (ET) sample, adsorption of *p*-TMPyP on LB (*m*) was carried out by a similar procedure described above. This sample is named as LB (*p* / *m*). Absorption spectra of LB (*m*), LB (*p*), and LB (*p* / *m*), where their loading levels are 40%, were measured as shown in Figure 5-7. It was found out that the spectrum for LB (*p* / *m*) (solid green line) is identical with a sum of individual absorption spectra of LB (*m*) and LB (*p*) (broken line). This indicates that there is no irregular interaction between *m*-TMPyP and *p*-TMPyP in the LB sample.

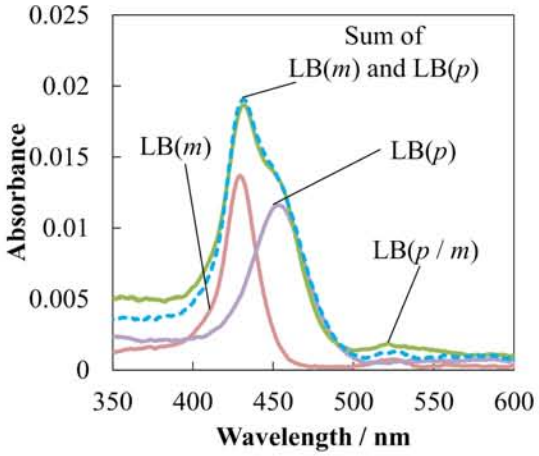


Figure 5-7. Absorption spectra of LB (*m*) (40% vs. CEC: red line), LB (*p*) (40% vs. CEC: purple line), and LB (*p* / *m*) (each 40% vs. CEC: green line) in water. Blue broken line indicates the sum of LB (*m*) and LB (*p*).

Fluorescence spectra of LB (*p* / *m*), where loading level of *m*-TMPyP and *p*-TMPyP are 40 and 40% vs. CEC, respectively, were measured. Excitation wavelength was set at 428 nm that is $\lambda_{max}$ of *m*-TMPyP. Fluorescence spectra of LB (*m*), LB (*p*), and LB (*p* / *m*) are shown in Figure 5-8.

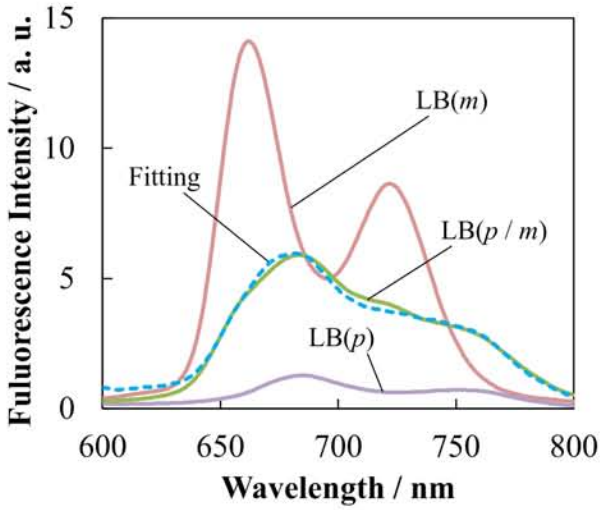


Figure 5-8. Fluorescence spectra of LB (*m*) (40% vs. CEC: red line), LB (*p*) (40% vs. CEC: purple line), and LB (*p* / *m*) (both *m*-TMPyP and *p*-TMPyP are 40% vs CEC: green line) in water. Blue broken line indicates the linear combination fitting curve using the fluorescence of LB (*m*) and LB (*p*).

In energy transfer sample LB (*p* / *m*), fluorescence from *m*-TMPyP (energy donor) decreased and that from *p*-TMPyP (energy acceptor) increased, compared to each reference sample (LB (*m*) and LB (*p*)). This clearly indicates that photochemical energy transfer reaction takes place between dyes at different layer in LB system. In a similar way, fluorescence spectra for LB (*p* / *m*), where loading level of *p*-TMPyP was 10, 20, 30% vs CEC, were measured. By using the fluorescence spectra of LB (*m*), LB (*p*), and LB (*p* / *m*), the energy transfer efficiency ($\eta_{ET}$) and the quenching efficiency ($\phi_q$) in energy

transfer sample LB ($p$ / $m$) can be calculated as follows. The total fluorescence of LB ($p$ / $m$) ($F_{ET}(\nu)$) can be expressed by equation (4-3).

On the basis of equation (4-3), the fluorescence spectrum $F_{ET}(\nu)$, was simulated with the respective reference fluorescence spectra, $F_D^0(\nu)$ and $F_A^0(\nu)$. Thus, parameters $\eta_{ET}$ and $\phi_q$ can be obtained from the spectral simulation and are summarized in Table 5-2.

Table 5-2. Energy Transfer Efficiency ($\eta_{ET}$) and Quenching Efficiency ($\varphi_q$) in LB ($p$ / $m$) Sample

| $p$-TMPyP (A) / $m$-TMPyP (D) | | $\eta_{ET}$ / % | $\varphi_q$ / % |
|---|---|---|---|
| Loading Level / % vs CEC | Adsorption density / molecules nm$^{-2}$ | | |
| 10 / 40 | 0.04 / 0.16 | 50 | 0 |
| 20 / 40 | 0.08 / 0.16 | 68 | 5 |
| 30 / 40 | 0.12 / 0.16 | 71 | 9 |
| 40 / 40 | 0.16 / 0.16 | 85 | 0 |

As loading level of $p$-TMPyP increased, $\eta_{ET}$ increased. This is due to the increase of adjacent number of energy acceptor. For all sample, energy quenching efficiency was below 10%. When loading levels of $m$-TMPyP and $p$-TMPyP are each 40%, $\eta_{ET}$ reached to 85% and $\varphi_q$ was zero. Thus, it is turned out that anisotropic energy transfer in three-dimensional system was efficiently achieved.

### 5-2-4. Conclusion

In this study, clay-porphyrin membrane that is suitable for anisotropic energy transfer reaction was successfully prepared by a combination of Langmuir-Blodgett (LB) technique and Size-matching effect. In this membrane, both two types of porphyrin that is energy donor and acceptor do not aggregate despite of high density adsorption condition. It was turned out that efficient anisotropic energy transfer between porphyrin molecules at different layer proceeded with high efficiency (85%). Since it is easy to apply other type of energy donors or acceptors, this system could be promising for the construction of artificial LHS that can absorb wide wavelength range of sunlight.

# 6. Conclusion

## ・Efficient use of sunlight by using various dyes on the inorganic nano-sheet

The novel tetra cationic xanthene derivative (Fluorone) was synthesized and its photochemical behaviors with and without clay were investigated. Fluorone adsorbed on the clay surface up to 134% vs. CEC without an aggregation. It is found out that fluorescence properties such as $\phi_f$ and $\tau_s$ are intrinsically retained upon complex formation with clay. Tetra cationic pyrene derivative (Pyrene) was synthesized successfully. The luminescence behavior of Pyrene on the clay surface was investigated and the fluorescence quantum yield increased. The fluorescence quantum yield of Pyrene increased about 12 times by adsorption on the clay surface (0.03→0.36). Judging from the result of lifetime measurement, it was found that the fluorescence rate constant was increased. It is considered that this increase of the fluorescence rate constant is due to the fact that the first excited state, which was forbidden, became an allowed transition by adsorption on the clay surface.

As a result, the development of dyes which can be used as light-harvesting dye on the clay surface was succeeded.

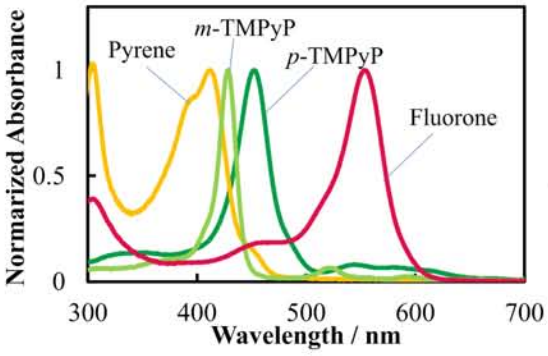


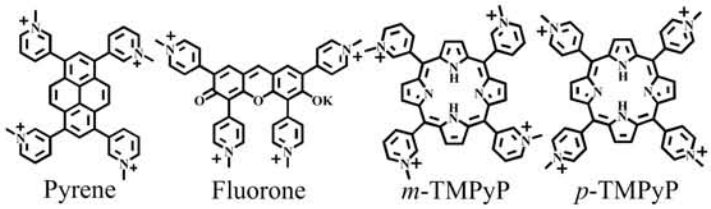

Next, the energy transfer reaction was investigated by using the three kind of dyes, which were Fluorone, *m*-TMPyP and *p*-TMPyP, on the clay surface. When [Fluorone] / [*p*-TMPyP] = 1, the efficiencies of the energy transfer reaction between Fluorone and *p*-TMPyP at 20-100% vs. CEC were larger than 90%. The maximum energy transfer efficiency was 99%. When the energy transfer reaction between Fluorone and *m*-TMPyP was evaluated, the energy transfer efficiencies were larger than 70% at [Fluorone] / [*m*-TMPyP] = 0.07 ~ 8. As a result, it was found out that energy transfer reactions from Fluorone to *m*-TMPyP and *p*-TMPyP were efficient.

Then, the quantitative excited singlet multiple-step energy transfer reaction among adsorbed three kinds of dyes on the clay surface was successfully achieved. Additionally, the energy transfer efficiencies of these multiple-step processes were analyzed using novel analysis formulae. The efficiency of energy transfer from Fluorone to *m*-TMPyP and *p*-TMPyP was 90% and from *m*-TMPyP to *p*-TMPyP was 75% when the total dye loading is 40% vs. CEC of the clay. Judging from these results, clay/porphyrin complexes are promising candidates as an efficient artificial LHS.

Additionally, we newly propose the parameter $\Gamma_{380\text{-}780\ nm}$ in order to evaluate the performance of the artificial LHS. $\Gamma_{380\text{-}780\ nm}$ indicates the ratio of the excitation frequency of energy acceptor in LHS to it without energy donor by sunlight irradiation. In the present system, $\Gamma_{380\text{-}780\ nm}$ was calculated to be 2.4 and we achieved to increase the excitation frequency of energy acceptor with using this artificial LHS.

## ・Concentration of sunlight by long range and anisotropic energy transfer

The photochemical energy transfer reaction on the clay surface between Fluorone and *p*-TMPyP was investigated. When [Fluorone]/[*p*-TMPyP] = 15, the energy transfer efficiency ($\eta_{ET}$) was still 80%, despite of a less amount of *p*-TMPyP. Judging from this observed $\eta_{ET}$ and theoretically calculated one, the occurrence of long range energy transfer reactions due to the energy migration between Fluorone molecules is expected. Fluorescence anisotropy observation of Fluorone supported this speculation. In this study, we found out that the efficient light harvesting type energy transfer system that equips the energy migration functionality can be constructed by using the system where J values between donor-donor and donor-acceptor are large. The concept obtained in this study can unfold options of strategies to construct the artificial light harvesting system that collects and concentrates the sunlight energy efficiently.

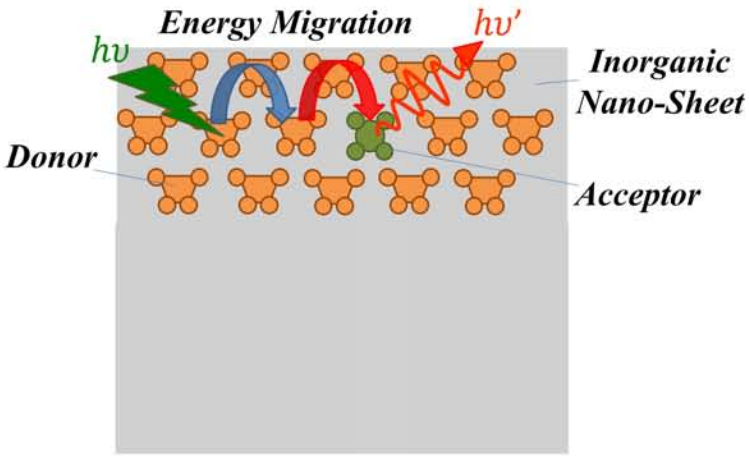

Next, clay-porphyrin membrane that is suitable for anisotropic energy transfer reaction was successfully prepared by a combination of Langmuir-Blodgett (LB) technique and Size-matching effect. In this membrane, both two types of porphyrin that is energy donor and acceptor do not aggregate despite of high density adsorption condition. It was turned out that efficient anisotropic energy transfer between porphyrin molecules at different layer proceeded with high efficiency (85%). Since it is easy to apply other type of energy donors or acceptors, this system could be promising for the construction of artificial LHS that can absorb wide wavelength range of sunlight.

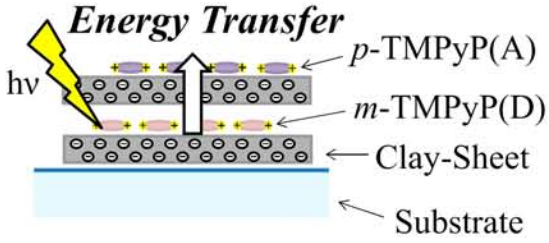

# 7. Reference


1. Scholes, G. D.; Fleming, G. R.; Olaya-Castro, A. and Grondelle, R. V. Lessons from Nature about Solar Light Harvesting. *Nature chemistry*, **2011**, *3*, 763-774.

2. Kirmaier, C. and Holten, D. Primary Photochemistry of Reaction Centers from the Photosynthetic Purple Bacteria. *Photosynthesis Research*, **1987**, *13*, 225-260.

3. Umena, Y.; Kawakami, K.; Shen. J. R. and Kamiya, N. Crystal Structure of Oxygen-Evolving Photosystem II at a resolution of 1.9 Å. *Nature*, **2011**, *473*, 55-60.

4. Fassioli, F.; Olaya-Castro, A.; Scheuring, S.; Sturgis, J. N. and Johnson, N. F. Energy Transfer in Light-Adapted Photosynthetic Membranes: from Active to Saturated Photosynthesis. *Biophysical Journal*, **2009**, *97*, 2464-2473.

5. Mcdermott, G.; Prince, S. M.; Freer, A. A.; Hawthornthwaite-Lawless, A. M.; Papiz, M. Z.; Cogdell, R. J.; Isaacs, N. W. Crystal Structure of an Integral Membrane Light-Harvesting Complex from Photosynthetic Bacteria. *Nature*, **1995**, *374*, 517–521.

6. Herek, J. L.; Wohlleben, W.; Cogdell, R. J.; Zeidler, D. and Motzkus, M. Quantum Control of Energy Flow in Light Harvesting. *Nature*, **2002**, *417*, 533-535.

7. Frank, H. A. and Cogdell, R. J. Carotenoids in Photosynthesis, *Photochemistry and Photobiology*, **1996**, *63*, 257-264

8. Macpherson, A. N.; Arellano, J. B.; Fraser, N. J.; Cogdell, R. J. and Gillbro, T. Efficient Energy Transfer from the Carotenoid $S_2$ State in a Photosynthetic Light-Harvesting Complex, *Biophysical*

*Journal*, **2001**, *80*, 923-930

9. Kirmaier, C. and Holten, D. Primary photochemistry of reaction centers from the photosynthetic purple bacteria, *Photosynthesis Research*, **1987**, *13*, 225-260
10. Fleming, G. R. and Scholes, G. D. Quantum mechanics for plants, *Nature*, **2004**, *431*, 256-257.
11. Bolton, J. R.; Stricker, S. J.; Connolly, J. S. Limiting and Realizable Efficiencies of Solar Photolysis of Water. *Nature*, **1985**, *316*, 495-500.
12. Inoue, H.; Shimada, T.; Kou, Y.; Nabetani, Y.; Masui, D.; Takagi, S. and Tachibana, H. The water oxidation bottleneck in artificial photosynthesis: How can we get through it? An alternative route involving a two-electron process, *Chem Sus Chem*, **2011**, *4*, 173-179
13. Miyatake, T.; Tamiaki, H.; Holzwarth, A. R.; Schaffner, K.Artificial Light-Harvesting Antennae: Singlet Excitation Energy Transfer from Zinc Chlorin Aggregate to Bacteriochlorin in Homogeneous Hexane Solution. *Photochem. Photobiol.* **1999**, *69*, 448-456.
14. Kim, D. and Osuka, A. Directly linked porphyrin arrays with tunable excitonic interactions, *Accounts of chemical research*, **2004**, *37*, 735-745
15. Panda, M. K.; Ladomenou, K. and Coutsolelos, A. G. *Coordination Chem. Reviews*, **2012**, *256*, 2601-2627.
16. Choi, M. S.; Aida, T.; Yamazaki, T. and Yamazaki, I. Dendritic multiporphyrin arrays as light-harvesting antennae: Effects of generation number and morphology on intramolecular energy transfer, *Chem. Eur. J.* **2002**, *8*, 2668-2678.

17. Kuznetz, O.; Davis, D.; Salman, H.; Eichen, Y. and Speiser, S. Intramolecular electronic energy transfer in rhodamine-azulene bichromophoric molecule, *Journal of Photochemistry and Photobiology A: Chemistry*, **2007**, *191*, 176-181

18. Leonardi, M. J.; Topka, M. R. and Dinolfo, P. H. Efficient Förster resonance energy transfer in 1, 2, 3-Triazole linked BODIPY-Zn(II) meso-tetraphenylporphyrin donor-acceptor arrays, *Inorganic chemistry*, **2012**, *51*, 13114-13122

19. Kim, D. and Osuka, A. Directly linked porphyrin arrays with tunable excitonic interactions, *Accounts of chemical research*, **2004**, *37*, 735-745

20. Panda, M. K.; Ladomenou, K. and Coutsolelos, A. G. *Coordination Chem. Reviews*, **2012**, *256*, 2601-2627.

21. Choi, M. S.; Aida, T.; Yamazaki, T. and Yamazaki, I. Dendritic multiporphyrin arrays as light-harvesting antennae: Effects of generation number and morphology on intramolecular energy transfer, *Chem. Eur. J.* **2002**, *8*, 2668-2678.

22. Hwang, I. W.; Park, M.; Ahn, T. K.; Yoon, Z. S.; Ko, D. M.; Kim, D.; Ito, F.; Ishibashi, Y.; Khan, S. R.; Nagasawa, Y.; Miyasaka, H.; Ikeda, C.; Takahashi, R.; Ogawa, K.; Satake, A. and Kobuke, Y. Excitation-energy migration in self-assembled cyclic zinc(II)-porphyrin arrays: A close mimicry of a natural light-harvesting system, *Chem. Eur. J.*, **2005**, *11*, 3753-3761.

23. Inagaki, S.; Ohtani, O.; Goto, Y.; Okamoto, K.; Ikai, M.;Yamanaka, K.; Tani, T.; Okada, T. Light Harvesting by a Periodic Mesoporous Organosilica Chromophore. *Angew. Chem., Ind. Ed.* **2009**,

*48*, 4042-4046.

24. Yamamoto, Y.; Takeda, H.; Yui, T.; Ueda, Y.; Koike, K.; Inagaki, S. and Ishitani, O. Efficient light harvesting via sequential two-step energy accumulation using a Ru-$Re_5$ multinuclear complex incorporated into periodic mesoporous organosilica, *Chemical Science,* **2014**, *5*, 639-648
25. "Introduction of Photochemistry", N. Mataga et al., Kyoritsu Shuppan Co., Ltd., 1975
26. Gfeller et al. 1997, JPCB
27. The Clay Science Society of Japan "Handbook of Clays and Clay Minerals, Third ed." 2009.
28. Okada, T.; Ide, Y.; Ogawa, M.; Oraganic-Inorganic Hybrids Based on Ultrathin Oxide Layers: Designed Nanostructures for Molecular Recongnition. *Chem. Asian J.* **2012**, *7*, 1980-1992.
29. S. Takagi, D.A. Tryk, H.J. Inoue, Photochemical Energy Transfer of Cationic Porphyrin Complexes on Clay Surface. *J. Phys. Chem. B.* **2002**, *106*, 5455-5460.
30. Takagi, S.; Eguchi, M.; Tryk, D. A.; Inoue, H. Light-Harvesting Energy Transfer and Subsequent Electron Transfer of Cationic Porphyrin Complexes on Clay Surfaces. *Langmuir*, **2006**, *22*, 1406-1408.
31. Ishida, Y.; Shimada, T.; Masui, D.; Tachibana, H.; Inoue, H.; Takagi, S. Efficient Excited Energy Transfer Reaction in Clay/ Porphyrin Complex toward an Artificial Light-Harvesting System. *J. Am. Chem. Soc.* **2011**, *133*, 14280-14286.
32. Ohtani, Y.; Shimada, T.; Takagi, S. Artificial Light-Harvesting System with Energy Migration Functionality in a Cationic Dye/Inorganic Nanosheet Complex. *J. Phys. Chem. C* **2015**, *119*,

18896-18902.

33. Boháč, P.; Crímerová, A.; Bujdák, J.; Enhanced Luminescence of 3, 3'-diethyl-2, 2'-thiacyanine Cations Adsorbed on Saponite Particles. *Applied Clay Sci.* **2016**, *127-128*, 64-69.

34. Takagi, S.; Shimada, T.; Ishida, Y.; Fujimura, T.; Masui, D.; Tachibana, H.; Eguchi, M.; Inoue, H.; Size-Matching Effect on Inorganic Nanosheets: Control of Distance, Alignment, and Orientation of Molecular Adsorption as a Bottom-Up Methodology for Nanomaterials. *Langmuir*, **2013**, *29*, 2108-2119.

35. Takagi, S.; Shimada, T.; Yui, T.; Inoue, H. High Density Adsorption of Porphyrins onto Clay Layer without Aggregation: Characterization of Smectite-Cationic Porphyrin Complex. *Chem. Lett.* **2001**, *30*, 128-129.

36. Ohtani, Y.; Ishida, Y.; Ando, Y.; Tachibana, H.; Shimada, T.; Takagi, S. Adsorption and Photochemical Behaviors of the Novel Cationic Xanthene Derivative on the Clay Surface. *Tetrahedron Letters*, **2014**, *55*, 1024-1027.

37. Ishida, Y.; Shimada, T.; Tachibana, H.; Inoue, H.; Takagi, S. Regulation of the Collisional Self-Quenching of Fluorescence in Clay/Porphyrin Complex by Strong Host-Guest Interaction. *J. Phys. Chem. A* **2012**, *116*, 12065-12072.

38. Götz, M.; Hess, S.; Beste, G.; Skerra, A.; Michel Beyerle, M. E. *Biochemistry* **2002**, *41*, 4156-4164.

39. Van Dao, L. *J. Luminescence* **2004**, *106*, 243-252.

40. López Arbeloa, F.; Tapia Estévez M. J.; López Arbeloa, T.; López Arbeloa, I. *Langmuir* **1995**, *11*, 3211-3217.

41. Tapia Estévez, M. J.; López Arbeloa, F.; López Arbeloa, T.; López Arbeloa, I. *J. Col. Int. Sci.* **1994**, *162*, 412-417.

42. Tapia Estévez, M. J.; López Arbeloa, F.; López Arbeloa, T.; López Arbeloa, I. *J. Col. Int. Sci.* **1995**, *171*, 439-445.

43. López Arbeloa, F.; Martínez Martínez, V.; Arbeloa, T.; López Arbeloa I. *J. Photochem. Photobiol. C: Photochem. Reviews* **2007**, *8*, 85-108.

44. Sasai, R.; Itoh, T.; Ohmori, W.; Itoh, H.; Kusunoki, M. *J. Phys. Chem. C* **2009**, *113*, 415-421.

45. Sasai, R.; Iyi, N.; Fujita, T.; López Arbeloa F.; Martínez Martínez, V.; Takagi, K.; Itoh, H. *Langmuir* **2004**, *20*, 4715-4719.

46. Bujdák, J.; Iyi, N.; Sasai, R. *J. Phys. Chem. B* **2004**, *108*, 4470-4477.

47. Kubin, R. F.; Fletcher, A. N. *J. Luminescence* **1982**, *27*, 455–462

48. Förster, T. Delocalized Excitation and Excitation Transfer. In *Mordern Quantum Chemistry*, Part III, Sinanoglu, O. Ed.; Academic Press: New York, 1965; 93-137.

49. http://pveducation.org/pvcdrom/appendices/standard-solar-spectra

50. T. Yui, T. Kameyama, T. Sasaki, T. Trimoto and K. Takagi, Pyrene-to-porphyrin excited singlet energy transfer in LBL-deposited LDH nanosheets, *J. Porphyrins and Phthalocyanines*, 11 (2007) 428-433.

51. H. Sato, K. Tamura, K. Ohara and S. Nagaoka, Multi-emitting properties of hybrid Langmuir-Blodgett films of amphiphilic iridium complexes and the exfoliated nanosheets of saponite clay, 38 (2014) 132-139.

52. K. Inukai, Y. Hotta, M. Taniguchi, S. Tomura and A. Yamagishi, J. Chem. Soc., Chem. Commun., (1994) 959

53. J. Kawamata, R. Seike, T. Higashi, Y. Inada, J. Sasaki, Y. Ogata, S. Tani and A. Yamagishi, Clay templating Langmuir-Blodgett films of a nonamphiphilic ruthenium(II) complex, Colloids and Surfaces A, 284-285 (2006) 135-139.

# Acknowledgement

I would like to express my gratitude to everyone for completing this doctoral thesis.

Prof. Shinsuke Takagi, a supervisor, had discussions and meetings with me many times. I would like to thank for Prof. Takagi's advice.

Dr. Tetsuya Shimada taught me how to use time-resolved spectroscope and discussed the results of its time-resolved spectroscopic measurements and other general spectroscopic measurements.

Prof. Motowo Yamaguchi and Prof. Yuji Kubo were examiner and gave me many helpful advices.

Dr. Yohei Ishida, Dr. Takuya Fujimura and Dr. Takamasa Tsukamoto were seniors in our laboratory and taught me experimental technique.

This work was supported by the JSPS KAKENHI Grant-in-Aid for JSPS Research Fellows (no. 15J06785).

Finally, I would like to express my gratitude to Yumiko Ohtani, my mother, and other family.

2017. 3 Yuta Ohtani